

Investigating the Last Millennium Coulomb Stress Transfer in the Central Apennine Fault System (CAFS)



Key Points:

- Historical and instrumental seismicity: analysis of the seismic events in the Central Apennine Fault System (CAFS) over the past millennium
- The Coulomb stress transfer (CST) analysis demonstrates the key role of static stress transfer in fault activation and inhibition in central Italy
- Innovative 3D model enhances CST accuracy in CAFS, revealing complex fault interactions and stress dynamics

Correspondence to:

G. Valentini,
giorgio.valentini@unicam.it

Citation:

Valentini, G., Volatili, T., Galli, P., & Tondi, E. (2024). Investigating the last millennium Coulomb stress transfer in the Central Apennine Fault System (CAFS). *Tectonics*, 43, e2024TC008328. <https://doi.org/10.1029/2024TC008328>

Received 12 MAR 2024

Accepted 23 SEP 2024

Author Contributions:

Conceptualization: G. Valentini, P. Galli, E. Tondi

Data curation: G. Valentini, P. Galli, E. Tondi

Formal analysis: G. Valentini

Funding acquisition: E. Tondi

Investigation: G. Valentini

Methodology: G. Valentini

Project administration: T. Volatili, E. Tondi

Resources: G. Valentini, E. Tondi

Software: G. Valentini

Supervision: T. Volatili, P. Galli, E. Tondi



Validation: G. Valentini, T. Volatili, P. Galli, E. Tondi

Visualization: G. Valentini

Writing – original draft: G. Valentini

Writing – review & editing: G. Valentini, T. Volatili, P. Galli, E. Tondi

Writing – review & editing: G. Valentini, T. Volatili, P. Galli, E. Tondi

G. Valentini^{1,2} , T. Volatili¹, P. Galli^{3,4} , and E. Tondi^{1,2}

¹School of Science and Technology - Geology Division, University of Camerino, Camerino, Italy, ²Istituto Nazionale di Geofisica e Vulcanologia (INGV), Sezione di Sismologia e Tettonofisica, Camerino, Italy, ³Dipartimento Protezione Civile, Rome, Italy, ⁴Consiglio Nazionale delle Ricerche, Istituto di Geologia Ambientale e Geoingegneria, Rome, Italy

Abstract The Central Apennine Fault System (CAFS) characterizes an active tectonic region of significant importance, witnessing numerous destructive seismic events over the last millennia. Although numerous studies have underscored the role of Coulomb stress transfer (CST) in initiating some of the most catastrophic earthquakes, investigations focusing on its specific influence within the CAFS are limited. This research delves into a thorough examination of the effects of CST on both historical and instrumental seismic events of significant magnitude associated with the CAFS. We selected nine seismic events for the CST investigation, dating from 1279 CE to present. Beyond analyzing the static stress transfer for each individual seismic event, the cumulative CST of recent instrumental earthquakes was also examined to provide a comprehensive overview of the current stress scenario. Leveraging an innovative approach, faults were modeled adopting a variable strike three-dimensional elliptical shape, ensuring enhanced calculation accuracy. Significant findings emerge from the analysis: CST has played a pivotal role in either activating or inhibiting the faults of the CAFS over the centuries. Several examined instances showcase fault reactivation following increased transferred stress within relatively short time frames, while others highlight the inhibitory effect of stress shadows. Examining the differences in seismic moment release across three seismicity windows (the first one between 1300 and 1400, the second around 1700, and the last one from 1979 to 2016) reveals distinct periods of higher seismicity in the past millennium. The latter shows the lowest cumulative seismic moment, suggesting a potential seismic gap equivalent to a Mw 6.67 earthquake. Deepening our understanding of CST illuminates the role of fault interactions in past earthquake occurrences, offering valuable insights into forecasting potential future seismic sequences. This awareness is vital in crafting targeted seismic risk mitigation strategies, thereby safeguarding local communities from the profound consequences of earthquakes.

Plain Language Summary Over the last millennium, the Central Apennine Fault System (CAFS) in Italy generated devastating earthquakes. This research delves into how Coulomb stress transfer (CST) has influenced the occurrence of these earthquakes, either activating or inhibiting faults as demonstrated by numerous CST studies on major earthquakes worldwide (e.g., the San Andreas Fault, Japanese megathrusts, North Anatolian Fault). By analyzing nine seismic events from 1279 CE to the present, we found that the static stress transferred among faults played a pivotal role. Utilizing an innovative 3D model to represent the faults, we gained a better understanding of how they interact with each other and how stress is distributed in the surrounding crust. Some earthquakes increased stress on certain faults, leading to their reactivation within relatively short periods, while others created “stress shadows” that calmed seismic activity. This knowledge not only helps us understand past earthquakes, but also which faults are currently more prone to causing earthquakes, thus improving seismic risk mitigation strategies to protect local communities. This study sheds light on the complex interactions among faults in the central Apennines, offering valuable insights that can assist in planning and preventing future seismic disasters.

1. Introduction

The Central Apennine Fault System (CAFS, sensu Cello et al., 1997) is characterized by strong seismic activity ($6.0 < M_w < 7.0$). The CAFS is an integral component of a complex mosaic of active fault systems spanning the Apennine range, extending over 130 km between the intramontane, tectonic basins of Colfiorito and L'Aquila (Figure 1).

© 2024. The Author(s).

This is an open access article under the terms of the [Creative Commons Attribution License](https://creativecommons.org/licenses/by/4.0/), which permits use, distribution and reproduction in any medium, provided the original work is properly cited.

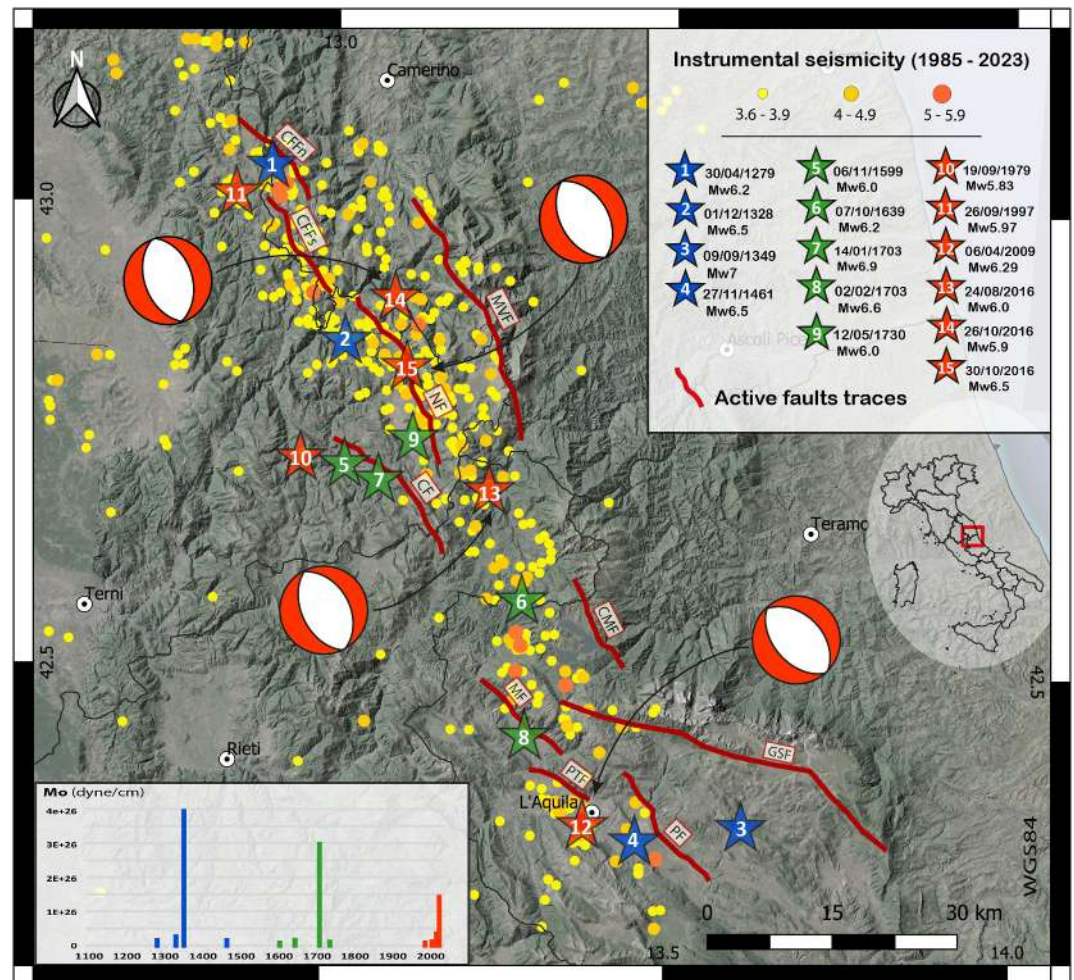


Figure 1. Map of the 15 seismic events with $5.8 \leq M_w \leq 7.0$ in the CAFS area since 1279 CE. Main active fault traces on the topographic surface are also shown in red (CFFn, Colfiorito Fault north; CFFs, Colfiorito Fault south; MVF, Monte Vettore Fault; NF, Norcia Fault; CF, Cascia Fault; CMF, Campotosto Fault; GSF, Gran Sasso Fault; MF, Marine Fault; PF, Paganica-San Demetrio Fault; PTF, Pettino Fault) (Galderisi & Galli, 2020; Galli, Galderisi, et al., 2022; Galli, Peronace, & Messina, 2022; Tondi, 2000; Tondi et al., 2020 and references therein). Modified after Valentini et al. (2023). Focal mechanism solutions are from Time Domain Moment Tensor (TDMT), INGV Data Set (Scognamiglio et al., 2006).

Since the Early Pleistocene, the central Italian Apennines have been subjected to an extensional tectonic regime oriented from northeast to southwest, leading to the formation of mainly NW-SE striking normal faults. In certain contexts, these have modified and overprinted pre-existing compressive structures, aligning with the genesis of the fold and thrust orogenic belt (Cello et al., 1997). This structural arrangement is composed of normal-oblique faulting, typically associated with the eastern margins of tectonic basins filled with sediments from the Late Pliocene-Early Pleistocene to Holocene (Boncio & Lavecchia, 2000; Boncio et al., 2004; Cello et al., 1995, 1997; Iezzi et al., 2019; Tondi, 2000; Tondi et al., 2020). The predominant NW-SE orientation of the CAFS fault planes mirrors the current stress field. The entire CAFS region displays evidence of Quaternary tectonic activity, as supported by several paleoseismological investigations (Blumetti, 1995; Falcucci et al., 2015; Galadini & Galli, 2003; Galderisi & Galli, 2020; Galli et al., 2005, 2008, 2011, 2018, 2023; Galli, Galderisi, et al., 2022; Galli, Peronace, & Messina, 2022; Iezzi et al., 2023) and by the occurrence of strong, crustal seismic events (CPTI15, 2023). Relying on the empirical relationship between fault length and magnitude outlined by Galli et al. (2008), the magnitude of the largest faults of the CAFS may range between $M_w 5.7$ and $M_w \sim 7.0$. These faults, with lengths ranging from a few kilometers to as long as 44 km, (e.g., the Gran Sasso Fault: Galli, Galderisi, et al., 2022), exhibit an average dip of ca. 55° . Several researchers have driven the detailed mapping of the fault scarps and the segmented surface traces of the CAFS, providing invaluable data for seismic risk assessments

(Barchi et al., 2000; Faure Walker et al., 2009, 2010, 2012; Galadini & Galli, 2000; Galli, Galderisi, et al., 2022; Galli, Peronace, & Messina, 2022; Mildon et al., 2017; Mildon, Roberts, et al., 2016; Morewood & Roberts, 2000; Papanikolaou & Roberts, 2007; Papanikolaou et al., 2005; Roberts, 2008; Roberts & Michetti, 2004; Tondi, 2000; Tondi et al., 2020; Wilkinson et al., 2015). However, in this study, we focus on the primary fault traces associated with the seismogenic sources, even though the surface expressions of these structures might be more articulated, with a segmented geometry, at a smaller observation scale.

Seismic and paleoseismic catalogs (CPTI15; Galli et al., 2008; Rovida et al., 2022) allow to infer that 15 earthquakes with magnitudes $M_w \geq 5.8$ that occurred in central Italy since 1279 AD can be attributed to the CAFS. Historical records highlight three distinct periods of strong seismic activity: the 12th–13th, 17th–18th, and 20th centuries onwards (Valentini et al., 2023). In the last few decades seismic occurrences were documented in the central Apennines, affecting the whole CAFS region, starting from the northernmost Colfiorito–Sellano sequence (1997, M_w 6.0) to the southernmost L’Aquila sequence (2009, M_w 6.2) (Amato et al., 1998; Chiarabba et al., 2009; Chiaraluce et al., 2011; Cello et al., 1998; Galli & Galadini, 1999; Tondi, 2000; Vittori et al., 2000; Vannoli et al., 2012). These seismic events resulted in substantial damage, leading to many casualties and displacing countless residents (Camassi et al., 1997; Galli et al., 2009).

The main challenge of this study is to understand how static stress transfer between the faults of the CAFS has influenced seismic sequences over the past 750 years and how it might affect future seismicity. Among the various mechanisms that can inhibit or promote fault rupture (Brodsky & van der Elst, 2014; Hetzel & Hampel, 2005; Oskin et al., 2008; Wedmore et al., 2017), Coulomb stress transfer (CST) played a key role in the past and likely continue to do so in the future, affecting earthquake recurrence time (Harris & Simpson, 1992; King et al., 1994; Reasenber & Simpson, 1992). King et al. (1994) demonstrated that part of the stress generated by a seismic event can be transferred to neighboring faults adjacent to the causative fault. Specifically, for faults with normal-to-oblique kinematics, the stress at the center of the causative fault (and generally at the slip zones) decreases instantaneously, transferring toward the fault tips and surrounding crust. This assumption has led many researchers (e.g., Galderisi & Galli, 2020; Improta et al., 2019; Mildon, Toda, et al., 2016, 2017; Mildon et al., 2019; Nostro et al., 2005; Pino et al., 2019; Wang et al., 2018; Wedmore et al., 2017) to examine the interaction among the faults of the central Apennines, given the presence of numerous active fault systems that have been activated over the last millennium, as evidenced by extensive historical catalogs. Additionally, previous studies have analyzed the cumulative CST on historical or instrumental seismic events outside the CAFS (e.g., Asayesh et al., 2020; Marchandon et al., 2021). However, the present study diverges in two fundamental aspects from previous research. The first one is related to the fault modeling approach; an elliptical geometry of the fault was factored into the CST calculations, and it appears to be particularly impactful in either increasing or decreasing stress at the ends of adjacent fault planes (Valentini et al., 2023). The second factor is the targeted analysis of CST on subsequently activated faults at potentially interactive distances and positions to isolate the effect of CST among earthquakes occurring in close spatiotemporal proximity. This study aims to analyze each considered earthquake individually and its effect in terms of CST on the subsequently activated fault. Here, a detailed analysis following step-by-step the CAFS seismic cycle progression to measure the influence of static stress culminates in an analysis of the cumulative stress derived from recent instrumental events.

Once the CST for each of the analyzed historical and instrumental earthquakes has been calculated, we seek to answer an intriguing scientific question that arose in a previous study (Valentini et al., 2023). The authors identify three prominent periods where most of the seismic moment was released. The initial phase spans from 1300 CE to 1400 CE, followed by a surge around 1700 CE, and the most recent phase extends from 1979 to 2016 with 300–350 years intervals. However, the scale of the released seismic moment varies across these distinct seismic periods. In the first seismicity window the cumulative seismic moment is approximately 1.35 times greater than in the second phase and about 2.31 times that of the third phase. Therefore, we hypothesize the existence of a notable seismic gap in the ongoing historical period. Should this gap exist, it implies the need for a seismic event large enough to bridge this gap. Studies regarding the connection between seismic gaps and CST have been provided by numerous authors who have demonstrated their direct correlation in various seismic regions worldwide (e.g., Alkan et al., 2023; Asayesh et al., 2020; Dong et al., 2022; Maleki Asayesh et al., 2019; Shan et al., 2013; Stein, 1999; Stein et al., 1997; Xiong et al., 2017). Therefore, CST calculation proves to be a valuable tool for understanding seismic sequences and potential seismic gaps, as well as providing insights into the most slip-prone causative faults. Finally, we will examine which faults could potentially bridge this seismic gap, in light of the CST analysis and the distribution of seismicity over the last millennium.

Table 1

List of Historical ($M_w \geq 6$) and Instrumental ($M_w \geq 5.8$) Seismic Events From 1279 to 2016 Caused by CAFS (From CPTI15; Rovida et al., 2022 and ISIDE Seismic Catalogs)

Year	Month	Day	Epicentral area	Lat	Lon	Io	Mw	ErrorMw	TMw	Source
1279	4	30	Colfiorito	43.093	12.872	9	6.20	0.16	Mdm	CPTI15
1328	12	4	Valnerina	42.857	13.018	10	6.49	0.28	Mdm	CPTI15
1349	9	9	Gran Sasso	42.334	13.613	10	~7.00	ND	Mdm	Galli, Galderisi, et al. (2022)
1461	11	27	L'Aquila	42.308	13.543	10	6.50	0.46	Mdm	CPTI15
1599	11	6	Cascia	42.724	13.021	9	6.07	0.24	Mdm	CPTI15
1639	10	7	Laga Mountains	42.639	13.261	9–10	6.21	0.15	Mdm	CPTI15
1703	1	14	Valnerina	42.708	13.071	11	6.92	0.1	Mdm	CPTI15
1703	2	2	L'Aquila	42.434	13.292	10	6.67	0.11	Mdm	CPTI15
1730	5	12	Valnerina	42.753	13.120	9	6.04	0.1	Mdm	CPTI15
1979	9	19	Valnerina	42.73	12.956	8–9	5.83	0.1	InsO	CPTI15
1997	9	26	Colfiorito	43.014	12.853	8–9	5.97	0.07	InsO	CPTI15/ISIDE
2009	4	6	L'Aquila	42.309	13.510	9–10	6.29	0.07	InsO	CPTI15/ISIDE
2016	8	24	Laga Mountains	42.698	13.233	10	6.00	0.07	InsO	CPTI15/ISIDE
2016	10	26	Valnerina	42.904	13.090		5.90	0.07	InsO	CPTI15/ISIDE
2016	10	30	Valnerina	42.83	13.109	11	6.50	0.07	InsO	CPTI15/ISIDE

Note. The seismic events selected for simulations are highlighted in green. “Lat” and “Lon” represent the coordinates of the epicenter, specifically Latitude and Longitude, respectively. “Io” denotes the epicentral intensity, and “Mw” refers to the moment magnitude along with the associated error (“ErrorMw”). The type of data used for calculating Mw is indicated in the “TMw” column: “Mdm” signifies that the data is derived from macroseismic intensities, while “InsO” indicates that the data is instrumental.

2. Seismicity and Fault Data

The initial step in our methodology involved the development of a basemap using a Geographic Information System (GIS). The database was populated with both tectonic and seismological information, serving dual purposes: first, for the selection of seismic events to be analyzed, and second, as the foundation for subsequent computational tasks.

Upon a comprehensive review of the available data, seismic events were selected for analysis based on their spatiotemporal proximity to subsequent events. The three-dimensional fault modeling, geared toward Coulomb stress calculations, was performed following the approach developed in Valentini et al. (2023). This approach considers the elliptical geometry of the fault plane as the most realistic representation, favoring the accuracy of the results.

The CPTI15 catalog documents 15 seismic events that have occurred within the boundary of the region affected by the CAFS, all with $M_w > 6.0$, spanning from 1279 CE to present day. By evaluating both the magnitude and the proximity to other fault that ruptured shortly after the primary event, we have chosen to focus on nine of these earthquakes in relation to the CST. The comprehensive list of these earthquakes, along with their specific attributes, is presented in Table 1, highlighting the ones selected for the CST analysis. For the multiple 1349 CE event we updated the catalog parameters based on the recent findings by Galli, Galderisi, et al. (2022) who identified the seismogenic source of its northern mainshock, assigning a $M_w \sim 7$.

Subsequently, through a review of the available literature on faults, including paleoseismological analysis, geological structures, and macroseismic observations, we associated a causative fault for each earthquake event. Fault traces were mapped and digitalized using a GIS, as depicted in Figure 1. This process was grounded in robust and well-established data from original geological studies (Barchi et al., 2000; Galadini & Galli, 2000; Galadini & Messina, 2001; Galderisi & Galli, 2020; Galli & Galadini, 1999; Galli et al., 2005, 2010, 2011, 2016, 2018; Galli, Galderisi, et al., 2022; Galli, Galderisi, Marinelli, et al., 2019; Galli, Galderisi, Peronace, et al., 2019; Galli, Peronace, & Messina, 2022; Messina et al., 2002; Tondi, 2000; Tondi & Cello, 2003; Tondi et al., 2020 and

Table 2
List of Causative Faults Belonging to the CAFS With Related Parameters From Barchi et al. (2000), Galli et al. (2010), ITHACA Working Group (2019), Galderisi and Galli (2020), Galli, Galderisi, et al. (2022), and Galli, Peronace, and Messina (2022)

Fault	Surface length (km)	Max subsurface length (km)	Dip angle	Dip direction	Rake
COLFIORITO NORD	8.9	19	50	230	−80
COLFIORITO SUD	12.8	17	50	236	−83
GRAN SASSO	44.4	60	63	208	−95
PAGANICA-SAN DEMETRIO	16.6	25	56	230	−97
CASCIA	19.5	27	61	230	−66
CAMPOTOSTO	8.4	12	51	249	−86
NORCIA	22.9	31	59	243	−64
VETTORE	34.4	54	68	240	−80
PETTINO	7.6	10	63	200	−95
MARINE	6.6	9	56	226	−97

Note. “Surface length (km)” and “Max subsurface length (km)” have been respectively measured from the fault traces on the map and calculated based on the elliptical shape with a major to minor axis ratio of 3:2.

references therein). Our fault database (Table 2) encompasses six fields such as: (a) fault name, (b) surface length, (c) subsurface length, (d) dip angle, (e) dip direction, (f) rake (using the Aki and Richards (1980) conventions).

3. CST Analysis

Within the framework of our research, we have operated under the assumption that subsequent to seismic activity on a specific fault, Coulomb stress can propagate to neighboring faults. If this stress is positive, it might encourage fault rupture, whereas if negative, it could deter it (King et al., 1994). Numerous factors, including the distance between the causative fault and its neighboring one, their shapes, positions, dynamics, and the slip of the source fault, influence the Coulomb stress changes. Utilizing the “Coulomb 3.4” software, we derived the CST using the equation (Lin & Stein, 2004; Toda et al., 2005):

$$\Delta\text{CST} = \Delta\tau_s + \mu\Delta\sigma_n$$

In this equation, ΔCST represents changes in CST, $\Delta\tau_s$ corresponds to changes in shear stress, while μ stands for the friction coefficient, and $\Delta\sigma_n$ signifies changes in normal stress. We adopted a friction coefficient of 0.6, which is appropriate for normal faults in the Central Apennines. This value balances theoretical models and empirical observations (Anderson, 1951; Byerlee, 1978; Collettini & Sibson, 2001; Fossen, 2016), making it suitable for CST analysis in this region (e.g., Galderisi & Galli, 2020). We also tested different values for the friction coefficient between 0.2 and 0.8 (extreme values not suitable for the rheologies and tectonic regime of the CAFS) but did not obtain significantly different results in terms of CST patterns. We opted for default spatial parameters with a Poisson's ratio of 0.25 and a Young's modulus of 800,000 bar.

Regarding the three-dimensional portrayal of faults within CST calculations, we leaned on the methodology proposed by Valentini et al. (2023). We integrated a three-dimensional model featuring strike variations and an elliptical shape into our CST algorithm, believing that an accurate representation of the CAFS is pivotal to reducing potential computational inaccuracies. In advancing with the CST simulations, we endeavored to mirror the real seismic rupture dynamics, factoring in variables such as the slip distribution or the partial or entire rupture.

To ensure sharp graphical detail and enhanced bar value precision, we established a 1 km grid for the fault modeling. Faults, perceived in an elastic half-space, were outlined as lines with variable strike and segmented into 1 km units. This intricate segmentation proved to be a balanced choice between output detail and modeling duration, deviating from the more typical practice of using 2 km segments for CST modeling. Subsequently, using the “Faults 3D” Matlab tool (Mildon, Toda, et al., 2016), we were able to construct 3D fault models, drawing from

actual traces and determining a slip distribution for each fault. We chose to compute the Coulomb stress for each fault segment, maintaining a consistent friction coefficient. Where available, we used actual slip data for recent earthquakes taken from the models in the database of finite-fault rupture models of past earthquakes (SRCMOD—Mai & Thingbaijam, 2014). For less documented seismic events, we assumed a centered slip distribution, reminiscent of a bull's eye pattern, depending on the relative seismic moment. In instances where the fault width was not specified in the reviewed literature, we used standard geometric relationships (Gupta & Scholz, 2000) to determine it, basing our calculations on a 1.5 aspect ratio (length/width). For faults with an extended length, their maximum depth was aligned with the thickness of the seismogenic layer, approximately 15 km (Chiarabba & De Gori, 2016; Gasparini et al., 1985). To optimize CST data comprehension, we crafted three distinct representations. Initially, a traditional CST map was produced at a depth of 5 km, in plain view, providing an approximation of CST distribution within the surrounding crust. This information was then translated to KML format for georeferenced visualization on Google Earth Pro®. Lastly, we crafted cross-sections perpendicular to fault strikes and developed a 3D model of the fault planes, obtaining the CST values for each 1 km fault segment, thus ensuring heightened precision in the assessment of stress for each individual segment.

4. Results

Here we present the outcomes of CST calculations undertaken for nine historical and instrumental earthquakes. As aforementioned, our primary objective is to determine the potential correlation between subsequent seismic events triggered by CST and the extent to which this phenomenon influences the rupture of neighboring faults. The selected earthquakes, chosen based on their seismic moment and proximity (both spatial and temporal) to subsequently activated faults, include:

1. Colfiorito earthquake, Mw 6.2 (30 April 1279);
2. Gran Sasso earthquake, Mw ~7.0 (09 September 1349);
3. Norcia and Cascia earthquake, Mw 6.92 (14 January 1703);
4. Upper Aterno earthquake, Mw 6.67 (02 February 1703);
5. Colfiorito earthquake, Mw 5.97 (26 September 1997);
6. Paganica earthquake, Mw 6.29, (06 April 2009);
7. Partial rupture at the southern tip of Mt. Vettore fault, Mw 6.00 (24 August 2016);
8. Partial rupture at the northern tip of Mt. Vettore fault, Mw 5.9 (26 October 2016);
9. Complete rupture of Mt. Vettore fault, Mw 6.5 (30 October 2016);
10. Cumulative CST generated by the 1997 Colfiorito, 2009 L'Aquila, and 2016 Vettore earthquakes.

Subsequent sections will delve into the specifics of how CSTs from the ruptured fault, “causative fault,” to the afterward activated fault, “receiver fault.” It is worth noting that despite our calculations are based on the best available data, there is still a significant lack of information regarding historical earthquakes (i.e., slip models, epicenter location, and magnitude), which implies an inherent uncertainty in the results obtained.

4.1. Colfiorito Earthquake (M_w 6.20, 30 April 1279) Versus Norcia Fault

We examined the 1279 CE earthquake that roughly occurred in the same region affected by the 1997 earthquake. This event was generated by the Colfiorito fault system, comprised of two primary structures: the Colfiorito north and south faults, here denoted as CFFn and CFFs. This fault system exhibits an en-echelon arrangement with a dextral step-over, as documented by Galli and Galadini (1999). According to these authors, the 1279 earthquake might share characteristics with the 1997 event, activating the same segments, especially Colfiorito north and south, which we modeled as a simultaneous rupture (Figure 2a). Nearly half a century later, in 1328, the Norcia fault (*sensu* Galli et al., 2018, 2023) experienced a rupture, leading to a Mw 6.49 earthquake (12 April 1328). This fault lies a few kilometers southeast of the Colfiorito fault system and has a similar orientation. Given the spatial and temporal proximity between the two earthquakes, we designated the parameters of the Norcia fault as a receiver fault and estimated the stress transfer induced by the 1279 earthquake.

This calculation considered planes with a dip direction of 243°, a dip angle of 59°, and a rake of −64°, as the Norcia fault. Our computational results in plain view (Figure 2a) reveal two prominent zones of negative stress, extending in opposing directions, toward the northeast and southwest, neither of which envelopes the CAFS faults. In turn, one positive stress lobe emanating from the fault tips of the causative Colfiorito faults targets the

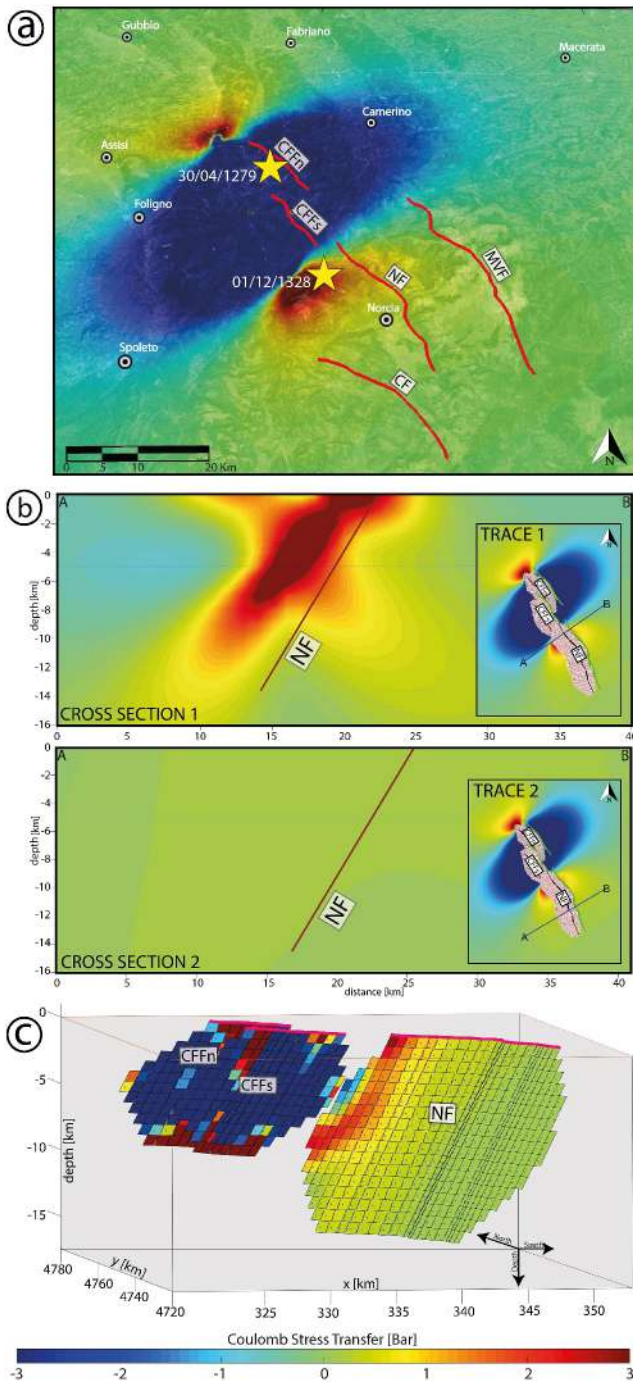


Figure 2. (a) Oblique view of the Coulomb stress transfer (CST) distribution on a plane located at a depth of 5 km. The causative faults are Colfiorito North and South, and the receiver fault is the Norcia Fault. (b) Cross-sections perpendicular to the receiver fault (NF) one at the northernmost part of the fault, near the causative fault and the other at the southern portion of the Norcia fault. Note the difference in the CST pattern when moving just a few kilometers away from the causative fault. (c) 3D view of the causative and receiver faults. Note that the CST is calculated on each of the rectangles that make up the entirety of the faults.

north-westernmost part of the Norcia fault, inducing a stress increase of up to 2 bars. The positive stress on the Norcia fault tends to wane rapidly moving southwards. Consequently, the northern part of the Norcia fault is more prone to rupture than its southern counterpart, which appears almost wholly unaffected, as highlighted in the three-dimensional stress modeling (Figure 2c). We constructed two parallel cross-sections, each approximately 40 km in length and perpendicular to the Norcia fault's orientation (Figure 2b). The second section is located roughly 18 km southeast of the first, near the Colfiorito fault system. The stress distribution within the crust exhibits notable variance when transitioning from the source fault, showing peak values of more than 3 bars in the first section and a maximum of 0.2 bars in the second.

4.2. Gran Sasso Earthquake ($M_w \sim 7.0$, 09 September 1349) Versus Paganica Fault

The 1349 earthquake, which impacted the southern part of our study area, stands out as the strongest seismic event in the historical records we reviewed. Galli, Galderisi, et al. (2022) ascertained that the causative fault for the northern mainshock of the 1349 seismic sequence was the Gran Sasso fault, a fault spanning 44 km. This earthquake, with a likely magnitude $M_w \sim 7.0$, damaged vast parts of central Italy, causing the partial collapse of some monuments in Rome. Given the fault segmented nature at the surface, we approached the seismic source as a unique, coherent unit. Over a century later, in 1461, a M_w 6.5 earthquake occurred in the hanging wall region of the Gran Sasso fault. This was attributed to the Paganica-San Demetrio fault (Galli et al., 2011), located roughly 10 km southwest of the Gran Sasso fault, representing thus a twin of the 2009 L'Aquila event, which was also sourced by this fault. Despite the considerable temporal gap between the two events, our choice to designate the Paganica fault as the receiver fault hinges on its proximity to the Gran Sasso Fault, a region frequently subject to stress shadows in typical CST scenarios between parallel faults. Our hypothesis finds support in the CST results at a 5 km depth in plain view (Figure 3a).

A pronounced stress shadow extends perpendicularly southwest from the fault strike, with the Paganica fault situated within this pronounced zone of stress diminution. Northeastwards, the stress shadow influence is expansive, evidenced by the blue lobe stretching nearly 80 km directly from the causative fault, underscoring the far-reaching impact of an earthquake of such scale on the neighboring crust. As is common with normal faults, the positive stress lobes are considerably more confined. Twin red lobes, emanating from the Gran Sasso fault deep terminations, project southeast and northwest. These lobes, registering stress increases exceeding 5 bars, span over 30 km in both directions and widen northeast-southwest as one distances from the causative fault. The plan view further reveals a conspicuous concentration of positive stress between the Gran Sasso and Paganica faults. This cluster signifies the deep root of a positive stress lobe, originating from a 5 km depth and reaching the surface, as the cross-section in Figure 3c displays. The plan view also shows positive stress lobes encompassing sections of the Marine, Pettino, and Campotosto faults. In contrast, the Paganica fault seems wholly enveloped in a stress shadow. Yet, cross-sectional analyses and 3D stress distribution (Figure 3b) depictions on fault planes reveal that the Paganica fault's super-

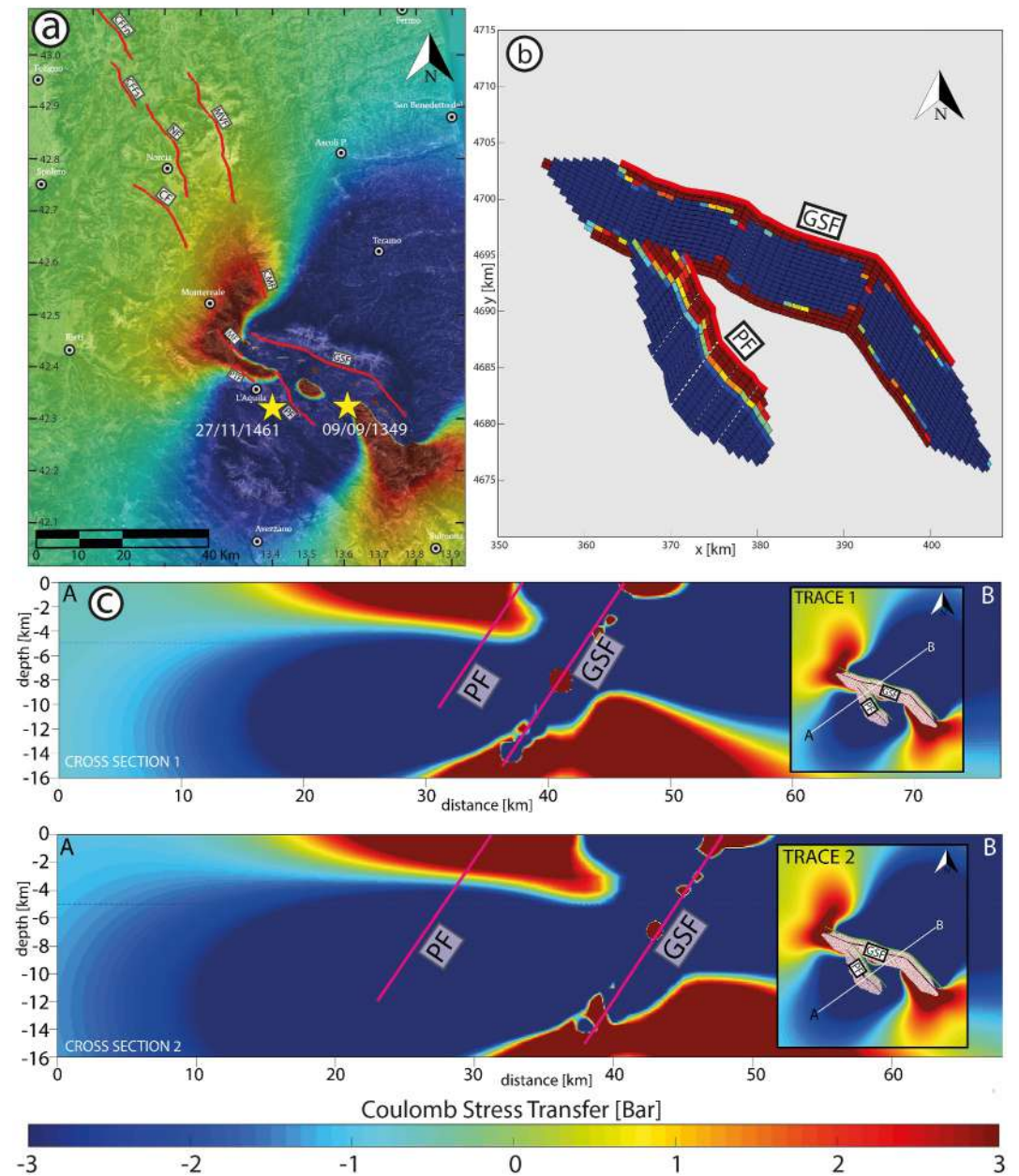


Figure 3. (a) Plan view of the Coulomb stress transfer (CST) distribution on a plane located at a depth of 5 km. The causative fault is the Gran Sasso Fault, and the receiver fault is the Paganica Fault. (b) 3D view of the causative and receiver faults. Note that the CST is calculated on each of the rectangles that make up the entirety of the faults. (c) Cross-sections perpendicular to the receiver fault (PF), one at the northernmost part of the fault and the other Cross-section at the southern portion of the Paganica fault.

ficial segment experiences up to 5 bars of positive stress transfer throughout its length, from the surface down to 5 km. Notably, this stress distribution remains largely consistent along the fault's strike. The upper cross-sectional representation in Figure 3c mirrors the lower one, positioned about 11 km further to the southeast. Conversely, the Gran Sasso fault exhibits a sharp stress reduction at the slip sites, typical of full fault ruptures where stress drops to zero. Nevertheless, the fault's extremities exhibit positive stress, as do the two marked bends dividing the fault into three segments with marginally distinct strikes. Additionally, it is worth noting that a minor positive stress magnitude (below 1 bar) reaches the southern extremities of the Monte Vettore, Norcia, and Cascia faults.

4.3. Norcia and Cascia Earthquake (M_w 6.92, 14 January 1703) Versus Paganica Fault

The Norcia Fault System (NFS), which includes the Cascia fault and Mt. Alvagnano fault (here considered as part of the CF; see Galderisi & Galli, 2020; Galli et al., 2018), has been responsible for some of the most powerful earthquakes in the western Mediterranean. Extending over a distance of 30 km, the NFS is composed of multiple interconnected segments. Like other fault systems found in the Apennines, the individual segments of the NFS have the capacity to rupture either independently or collectively, resulting in earthquakes of moderate to high intensity. However, catastrophic events occur only when the entire system (Norcia faults plus Cascia faults) undergoes rupture, as witnessed by the M_w 6.9 earthquake on 14 January 1703 (Galli, Peronace, & Messina, 2022). Shortly after the strong earthquake in Norcia, on 2 February 1703, another devastating earthquake (M_w 6.7) struck the upper Aterno Valley, causing widespread destruction of the surrounding villages, including L'Aquila (MCS 9). This seismic event affected an extensive area located approximately 40 km southeast of the fault responsible for the earthquake on January 14. The close spatial and temporal proximity of these two earthquakes makes them ideal for studying the interaction between the fault systems involved, specifically in terms of CST. Following the study by Galli et al. (2011), the receiver faults considered in this analysis are the Marine Fault, Pettino Fault, and Paganica-San Demetrio Fault (i.e., the Upper Aterno fault system in Galadini and Galli (2000)), all of which experienced rupture on 2 February 1703. It is worth noting that, once again, the rupture did not occur along a single fault but rather involved a series of segments that likely ruptured simultaneously (Moro et al., 2013). As can be inferred from Figure 4a, the area subjected to changes in Coulomb stress after the earthquake on 14 January is extensive. The two lobes of negative stress usually generated by slip on normal faults extend for tens of kilometers in the northeast-southwest direction, placing the Monte Vettore Fault (MVF) under a significant stress shadow zone.

Within the shadow zone, a few kilometers west of the CF, a spot of positive stress appears, likely generated at the northern tip of the CF, creating heterogeneity in the CST pattern. However, there is no active fault present in the positively stressed zone. Two large lobes of stress increase (up to 5 bars) extend northwest and southeast from the middle zone between the two causative faults. The stress increase toward the northwest largely involves the Colfiorito fault system, branching toward Fabriano and Foligno, creating the classic “butterfly wing” pattern. This latter shape is absent in the positive lobe that extends from the causative faults toward the southeast. Here, the extent of the positively stressed crustal area appears larger and reaches to influence the Campotosto fault (CMF) and the northern tip of the Marine fault (MF). A modest increase in Coulomb stress is also recorded on the Pettino fault (PTF) and the northern tip of the Gran Sasso fault. In these last two cases, the stress increases by no more than 0.8 bars. It follows that the only fault involved in the earthquake on 2 February 1703, which received a significant CST “push” from the earthquake of 14 January of the same year, is the Marine fault. In the cross section and three-dimensional modeling (Figures 4b and 4c), the northern tip of the Marine fault experiences an increase in stress of approximately 1 bar, gradually decreasing moving south along the fault. The Paganica fault, as shown in cross section 2, exhibits a slight stress increase of about 0.3 bar. Overall, the three receiver faults seem to have undergone a stress increase significantly lower than what would have been expected from an earthquake of such magnitude.

4.4. Upper Aterno Earthquake (M_w 6.67, 02 February 1703) Versus Norcia Fault

The last historical earthquake considered occurred days after the devastating earthquake that struck the Norcia area. On 2 February 1703, a probable cascading activation of three faults in the southern portion of the CAFS generated an earthquake with a magnitude of M_w 6.67. The causative faults were identified (Galli et al., 2011) as belonging to the Upper Aterno Fault System (Marine, Pettino, and Paganica-San Demetrio faults). Given their sizes, these individual faults would not be capable of producing such magnitude on their own. Thus, a simultaneous activation of the entire fault system is implicated. The subsequent earthquake occurred in 1730, 27 years later, involving the southern half of the Norcia fault, which had also been previously activated in 1703. This M_w 6.04 earthquake was taken as a reference to decide the receiver fault for this simulation. The plan view modeling in Figure 5a reveals a large stress shadow divided into two main lobes directed northeast and southwest. The first completely covers the Gran Sasso fault, depriving it of about 5 bars of stress. The Campotosto fault, especially its southern half, also underwent diminishing stress. The second lobe does not encompass any active and capable fault present in our study. The causative faults all lie within the stress shadow with localized spots of very high positive stress, which are not considered significant as the stress on the causative fault is assumed to reduce to zero after the stress drop due to its activation. Two lobes of positive stress radiate from the northern tip of the Marine

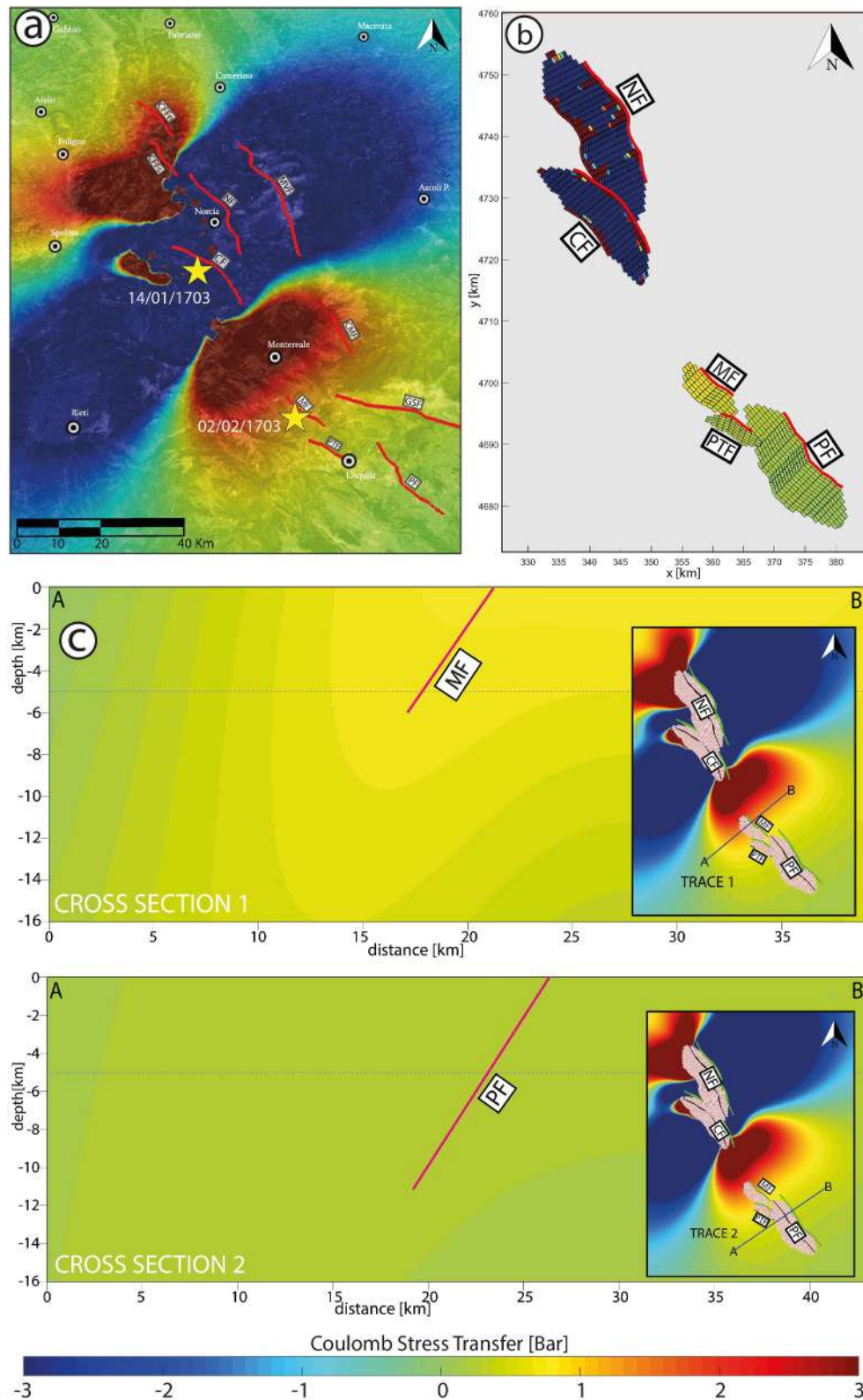


Figure 4. (a) Oblique view of the Coulomb stress transfer (CST) distribution on a plane located at a depth of 5 km. The causative faults belong to the Norcia Fault System and the receiver fault is the Paganica Fault. (b) 3D view of the causative and receiver faults. Note that the CST is calculated on each of the rectangles that make up the entirety of the faults. (c) Cross-sections perpendicular to the receiver faults (MF and PF), one at the northernmost part of the MF, near the causative faults and the other Cross-section on the PF. Note the difference in the CST pattern when moving just a few kilometers away from the causative fault.

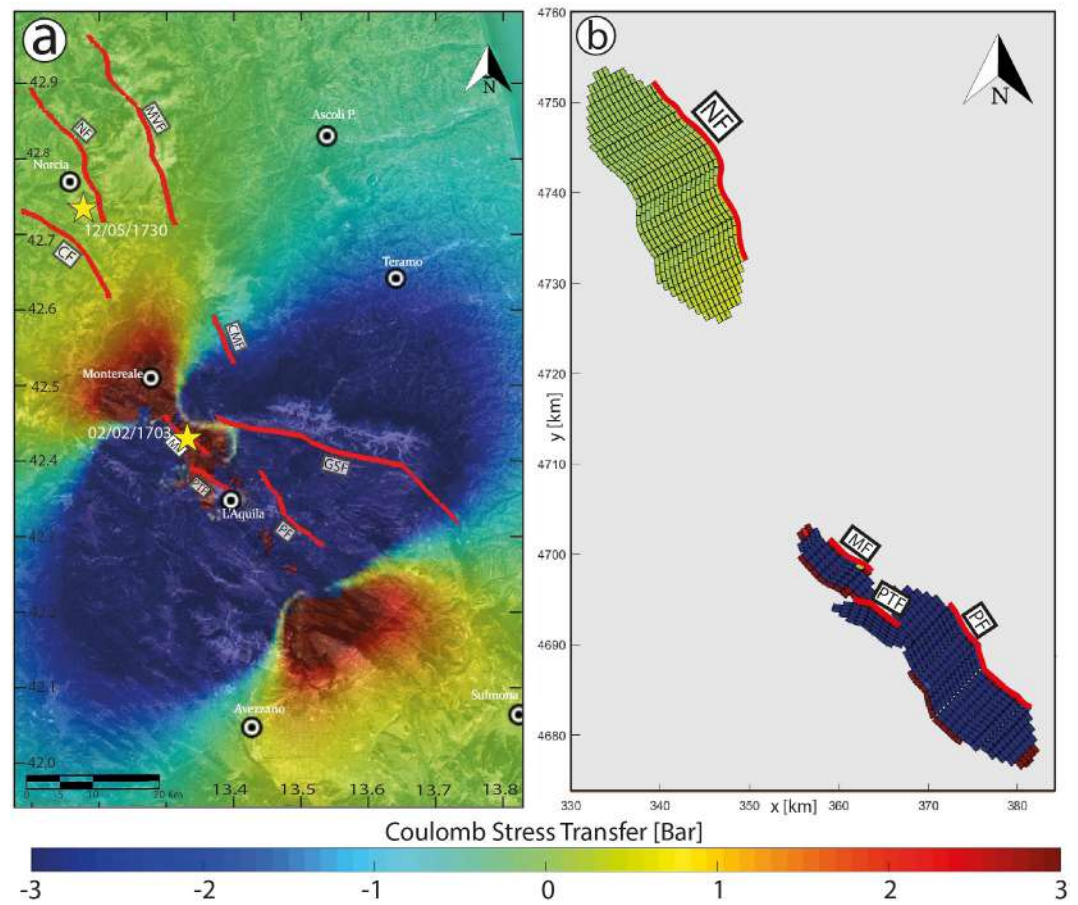


Figure 5. (a) Plan view of the Coulomb stress transfer (CST) distribution on a plane located at a depth of 5 km. The causative faults are the Marine, Pettino and Paganica-San Demetrio faults (Upper Aterno Fault System) and the receiver fault is the Norcia Fault. (b) 3D view of the causative and receiver faults. Note that the CST is calculated on each of the rectangles that make up the entirety of the faults.

fault northwestward and from the deep southern tip of the Paganica-San Demetrio fault southeastward. The first of these affects the southern half of the Cascia fault, transferring a maximum of 0.8 bars of positive stress. However, the next fault to activate was the Norcia fault, which received only 0.5 bars of positive stress exclusively at its southern tip. The minimal influence exerted by this earthquake on the Norcia fault is better seen in the three-dimensional modeling in Figure 5b. The Vettore fault also underwent a very modest stress transfer of about 0.5 bars, again only in the southern portion. The stress lobe branching from the Paganica-San Demetrio fault southward, however, has a greater extent, reaching the cities of Avezzano and Sulmona. Given the meager stress transfer to the receiver fault, it was deemed unnecessary to proceed with the creation of cross sections along that fault.

4.5. Colfiorito Earthquake (M_w 5.97, 26 September 1997) Versus Vettore Fault

The first earthquake considered from the instrumental catalogs is the 1997 earthquake that occurred in the Colfiorito Basin, in the northernmost part of the CAFS. This earthquake is considered analogous to the historical earthquake of 1279 (Galli & Galadini, 1999). Therefore, we modeled both earthquakes in the same manner, with the only difference being the generated seismic moment (and consequently, the slip), which is lower for the more recent earthquake. It should be noted that the inferred magnitude generated by the Colfiorito fault system in 1279 was M_w 6.2, while in 1997, the measured value for the 26 September mainshock was M_w 5.97. In addition to the mainshock, a series of closely spaced events occurred, all between the months of September and October. A foreshock with a magnitude of M_w 5.66 alerted the population at 00:33, causing many people to leave their homes, thereby limiting injuries and fatalities. At 9:40, the mainshock of M_w 5.97 occurred, followed by a M_w

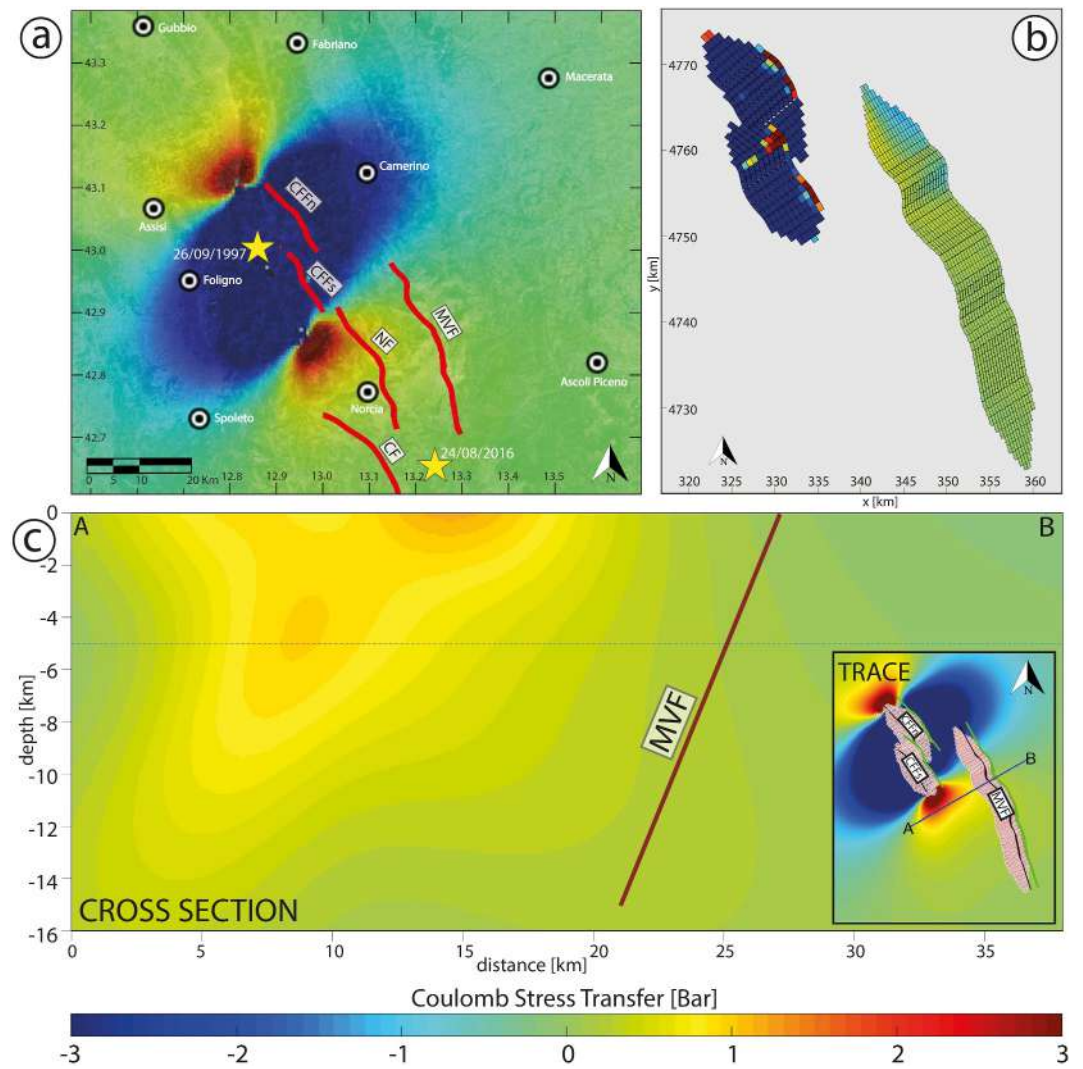


Figure 6. (a) Plan view of the cumulative Coulomb stress transfer (CST) distribution on a plane located at a depth of 5 km. The causative faults are Colfiorito North and South, and the receiver fault is the Mt. Vettore Fault. (b) 3D view of the causative and receiver faults. Note that the cumulative CST is calculated on each of the rectangles that make up the entirety of the faults. (c) Cross-section perpendicular to the receiver fault (MVF).

5.22 and a Mw 5.47 aftershocks. For this reason, it was appropriate to calculate the cumulative stress generated by all four major seismic events, resulting in a cumulative seismic moment of $1.92572E + 25$ dyne-cm, thereby approaching the seismic moment generated by the 1279 earthquake. The contribution of aftershocks and foreshocks in the overall CST framework resulted in only slight changes in the amount of stress (both positive and negative) transferred to the surrounding crust. Comparing the results of the 1279 and the 1997 earthquakes (see Section 4.1), it can be observed that a modest increase in slip or magnitude has an important influence on the amount of CST around the causative faults. In this simulation, the receiver fault is the Monte Vettore fault, which activated in 2016, causing three devastating earthquakes in close succession. The aim is to understand if the 1997 earthquake played a role in the subsequent activation of the MVF in 2016.

Figure 6a shows the cumulative stress pattern generated at a depth of 5 km by the simultaneous activation of CFFn and CFFs in the 1997 sequence on faults with the same rake and strike as the MVF. The stress shadow stands out compared to the zones of positive CST, extending almost symmetrically in the northeast-southwest direction. The two positive lobes seem to be positioned like those generated by the 1279 earthquake, with no significant differences in intensity and extent reaching a positive stress value of 3 bars. However, as depicted in Figures 6b and 6c, it is not enough to significantly influence the stress on the Monte Vettore fault, which remains almost

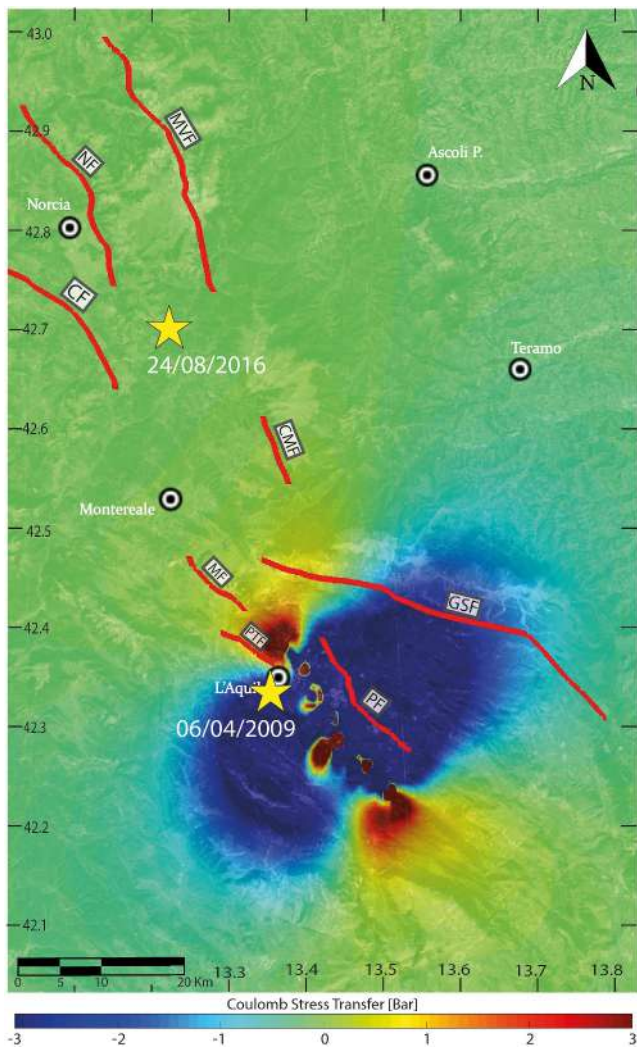


Figure 7. Plan view of the Coulomb stress transfer distribution on a plane located at a depth of 5 km. The causative fault is the Paganica-San Demetrio fault, and the receiver fault is the Mt. Vettore Fault.

unchanged, as if it had not been affected by the CST generated by the 1997 earthquake except in the northern tip, where the stress state depends on the fault depth. From 0 to 8 km depth, in the northern tip of the receiver fault, the effect of the stress shadow is clearly visible, with a stress reduction up to -1 bar. However, at greater depths in the same area, the Monte Vettore fault appears to have received modest positive stress (up to 0.4 bar). In Figure 6a, it can be seen that only the northern tip of the Norcia fault undergoes a substantial increase in stress of about 1.5 bars, but just a few kilometers away toward the MVF, this amount gradually decreases until it is almost negligible. The highest value of CST recorded on the MVF after the 1997 earthquake is only 0.4 bars. The same applies to the Cascia fault, of which only the northern tip is slightly influenced (0.2–0.4 bars) by the slip of the Colfiorito faults.

4.6. Paganica Earthquake (M_w 6.29, 06 April 2009) Versus Vettore Fault

On 6 April 2009, the Abruzzo city of L'Aquila was severely struck by a M_w 6.29 earthquake. The proximity of the epicenter to the city contributed to hundreds of casualties and significant buildings damages and collapses. The causative fault of this earthquake has been identified by several authors as the Paganica-San Demetrio fault (Anzidei et al., 2009; Chiaraluce, 2012; Cinti et al., 2011; EMERGEO Working Group, 2010; Galli et al., 2011; Pantosti & Boncio, 2012; Walters et al., 2009). This structure, spanning 16.6 km (at the surface), is an almost pure dip-slip fault and has generated at least two significant historical earthquakes (1461 and 1703). Just 7 years after the activation of the Paganica-San Demetrio fault, another earthquake struck an area located approximately 60 km to the north-northwest. The series of earthquakes that hit the central Apennines in 2016 were generated by the Monte Vettore fault, which had been silent for many centuries before (Galli, Galderisi, Marinelli, et al., 2019; Galli, Galderisi, Peronace, et al., 2019). At the surface, the Monte Vettore fault is about 34 km long and was capable of generating multiple events within a brief period. The seismic sequence produced an initial M_w 6.0 earthquake on 24 August 2016, followed by an M_w 5.9 on October 26. Finally, the most intense seismic event occurred on October 30, with a magnitude of M_w 6.5.

Given the brief time interval between the earthquake of 2009 and those of 2016, we are interested in understanding the potential influence of the activation of the Paganica-San Demetrio fault on the Monte Vettore fault.

As expected, the distance between the two faults and the moderate magnitude of the L'Aquila earthquake are factors that leave the Monte Vettore fault almost untouched by the stress transfer resulting from the activation of the Paganica-San Demetrio fault. As evident from the plan view modeling in Figure 7, the positive stress lobes extending from the fault tips toward the northwest and southeast have a limited extent of a few kilometers, partially embracing only the Marine and Pettino faults. Even the northwestern tip of the Gran Sasso fault receives moderately low positive stress (approximately 0.7 bar). Positive stress spots stand out as embedded within the stress shadow on the hanging wall of the causative normal fault, located about 4–5 km southwest of the surface trace. Toward the northeast, the stress shadow is more extensive and covers the central third of the Gran Sasso fault. On the other hand, toward the southwest, no faults are inhibited by the zone of decreased Coulomb stress.

The Monte Vettore fault, taken as the receiver fault in this calculation, experiences a stress transfer of no more than 0.2 bars, which is negligible. Three-dimensional analysis was not deemed necessary as the receiver fault did not show significant signs of stress transfer from the activation of the Paganica-San Demetrio fault, however, a cumulative three-dimensional modeling of all recent seismic events has been performed, as shown in Figure 11. Since the southern sector of the CAFS has recently only experienced the L'Aquila earthquake, this model can be

referred to for a three-dimensional visualization of CST on the faults surrounding the Paganica-San Demetrio fault.

4.7. The 2016 Mt. Vettore Fault Seismic Sequence

The last seismic event in the catalogs struck the central Apennines in 2016. The Mt. Vettore fault system, comprising dozens of surface segments with an en-echelon arrangement, generated three earthquakes within a little over 2 months. The main seismogenic structure experienced partial activation, first at the southern fault tip on 24 August (Mw 6.0), involving also the Amatrice fault, which is located along the strike to the south (in our model, it is integrated with the southern tip of the Mt. Vettore fault), then at the northern fault tip on 26 October (Mw 5.9), and finally, the central segment was activated, involving the two previously activated tips, resulting in a catastrophic earthquake of magnitude Mw 6.5.

In this section, we analyze the results obtained from the modeling of both the partial activation and the entire rupture of the Monte Vettore fault. In this case study, the receiver fault is the same as the causative fault, in fact we want to understand the influence that a partial rupture of one segment had on the remaining inactivated part of the fault. The objective is to determine if and how much the three subsequent events were driven by CST.

Regarding the complete rupture on 30 October, we will analyze the CST on the Norcia fault, which is in a precarious position relative to the Monte Vettore fault. The Norcia fault raises concern due to its size, its proximity to several inhabited areas, and the time elapsed since its last total reactivation in 1703 (Galli et al., 2023). In order, we will analyze:

1. The effect of the southern tip partial rupture on the central-northern portion of the fault.
2. The effect of the northern tip partial rupture on the central-southern portion of the fault.
3. The effect of the entire fault surface rupture on the surrounding crust and, in particular, on the Norcia fault.

On 24 August, when the southern tip of the Monte Vettore fault ruptured together with the northern tip of the Amatrice fault, it generated a wide stress shadow that partially affected the southernmost section of the Norcia fault and part of the Cascia fault, reducing stress by approximately 1 bar. The positive stress transfer involved two lobes radiating toward the northwest and southeast from the rupture surface (Figure 8a). The southern lobe did not affect any of the faults in the CAFS except for the Campotosto fault, which, however, experienced a negligible CST (around 0.2 bar). Of interest is the northern lobe of positive stress that involves part of the central section of the same fault. The sections in Figure 8c show that the locked zone of the fault closest to the ruptured portion, after 24 August, is highly stressed over its entire width, and then the imparted stress decreases drastically as it moves away from the southern tip. From the three-dimensional modeling in Figure 8b, this effect appears to be associated with a gentle bend at the boundary with the rupture. There is an accumulation of stress of up to 6 bars in the area confined between the end of the coseismic rupture and the hinge of the bend with the concavity facing southwest. However, the northern half of the fault seems untouched in terms of CST.

A similar and specular situation was obtained by modeling the partial activation of the northern segment ruptured on 26 October. The seismic moment generated was lower than the earthquake on 24 August, approximately $8.81049E + 24$ dyne-cm compared to $1.24451E + 25$ dyne-cm of the previous earthquake, resulting in reduced intensity and extent of both the positive stress lobes and the stress shadow (Figure 9a). The stress shadow weakly reaches the northwestern tip of the Norcia fault and the southeastern tip of the Colfiorito south fault, but with a stress reduction of about -0.4 bar. The positive lobes extend both toward the northwest and southeast, affecting the stress state of the southeastern tip of the Colfiorito fault, where the CST does not exceed 0.6 bars. The Monte Vettore fault experiences significant stress only in a narrow portion adjacent to the rupture zone. The two cross sections (Figure 9c) about 12 km apart from each other demonstrate how the CST is concentrated only in the area adjacent to the rupture, dissipating drastically as it moves southeastward. The three-dimensional modeling in Figure 9b reveals that the situation is remarkably similar to that anticipated from the modeling on 24 August. Positive stress is concentrated around a bend, more pronounced in this case, with the same concavity as the one to the south of the fault. Starting from the bend toward the southeast, the CST gradually tends to zero within a few kilometers, leaving the stress state of the central part of the fault almost unchanged.

On 30 October, a powerful seismic event originated from the activation of the central segment of the Monte Vettore fault system, concurrently reactivating its previously fractured northern and southern segments. The slip distribution for this comprehensive rupture exhibited an asymmetrical pattern, predominantly localized within the

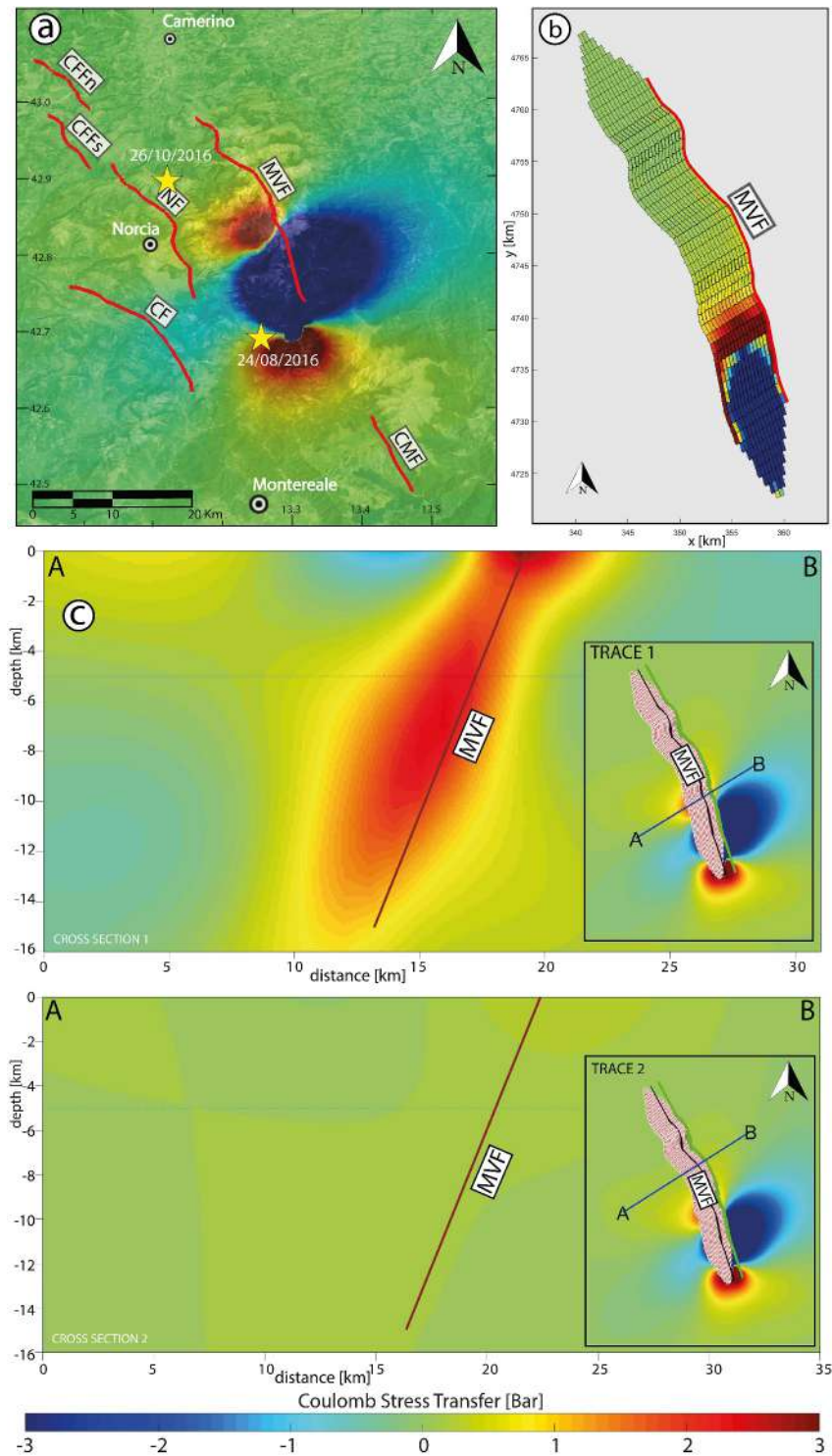


Figure 8. Coulomb stress transfer (CST) related to the 24 August 2016 earthquake. (a) Oblique view of the CST distribution on a plane located at a depth of 5 km. The causative fault is the southernmost portion of the Mt. Vettore Fault and the receiver is its central and northern portion. (b) 3D view of the CST on the Mt. Vettore Fault. Note that the CST is calculated on each of the rectangles that make up the entirety of the fault. (c) Cross-sections perpendicular to the MVF, one near the southern partial rupture and the other cross-section at the central portion of the MVF. Note the difference in the CST pattern when moving just a few kilometers away from the rupture.

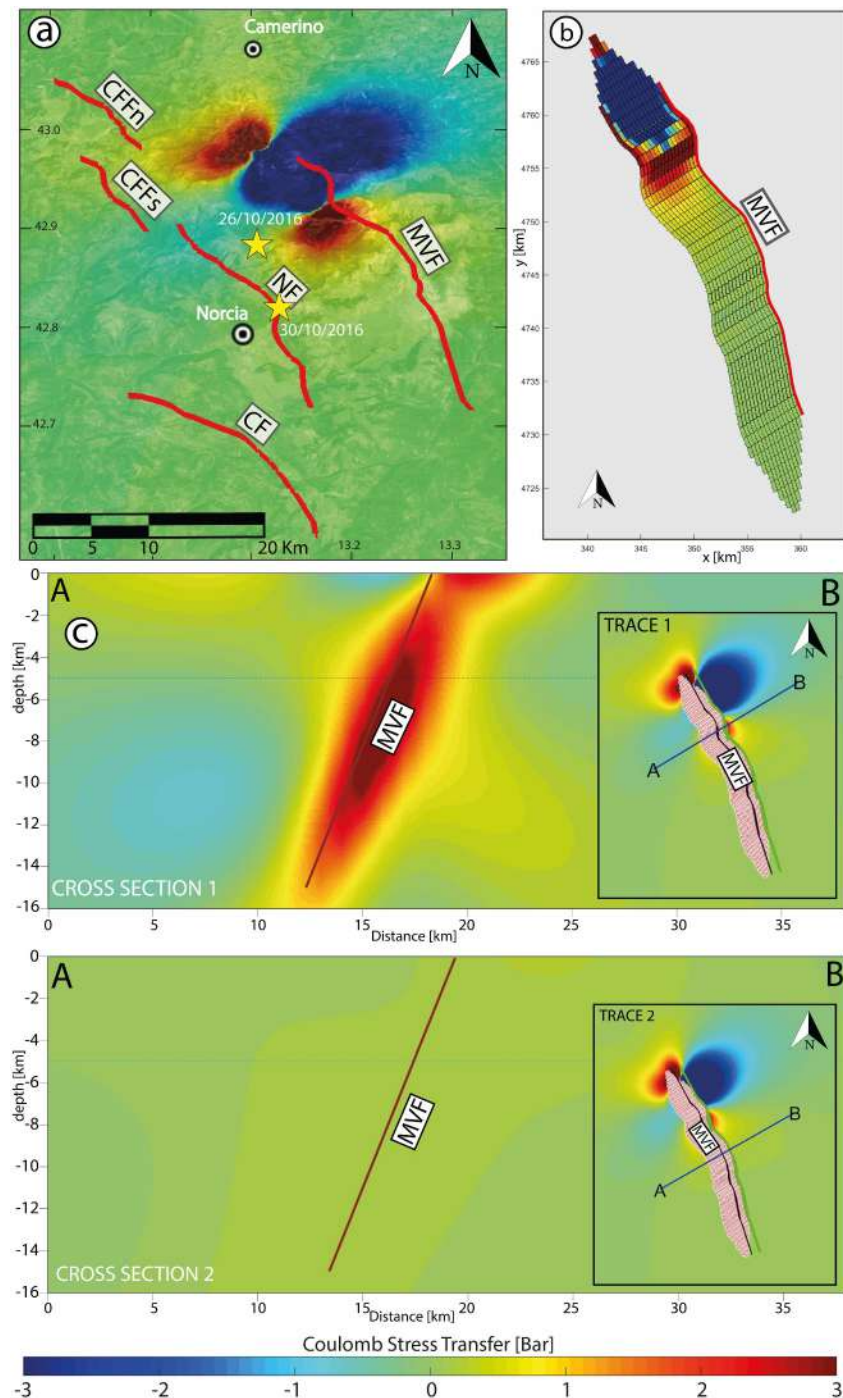


Figure 9. Coulomb stress transfer (CST) related to the 26 October 2016 earthquake. (a) Oblique view of the CST distribution on a plane located at a depth of 5 km. The causative fault is the northernmost portion of the Mt. Vettore Fault and the receiver is its central and southern portion. (b) 3D view of the CST on the Mt. Vettore Fault. Note that the CST is calculated on each of the rectangles that make up the entirety of the fault. (c) Cross-sections perpendicular to the MVF, one near the northern partial rupture and the other cross-section at the central portion of the MVF. Note the difference in the CST pattern when moving just a few kilometers away from the rupture.

southern third of the fault. The ensuing CST pattern is markedly larger and more heterogeneous (Figure 10a) when compared with prior two modeling attempts. Notably, the stress shadow enveloping the footwall is approximately five times broader than that observed over the hanging wall. The latter induces a significant stress

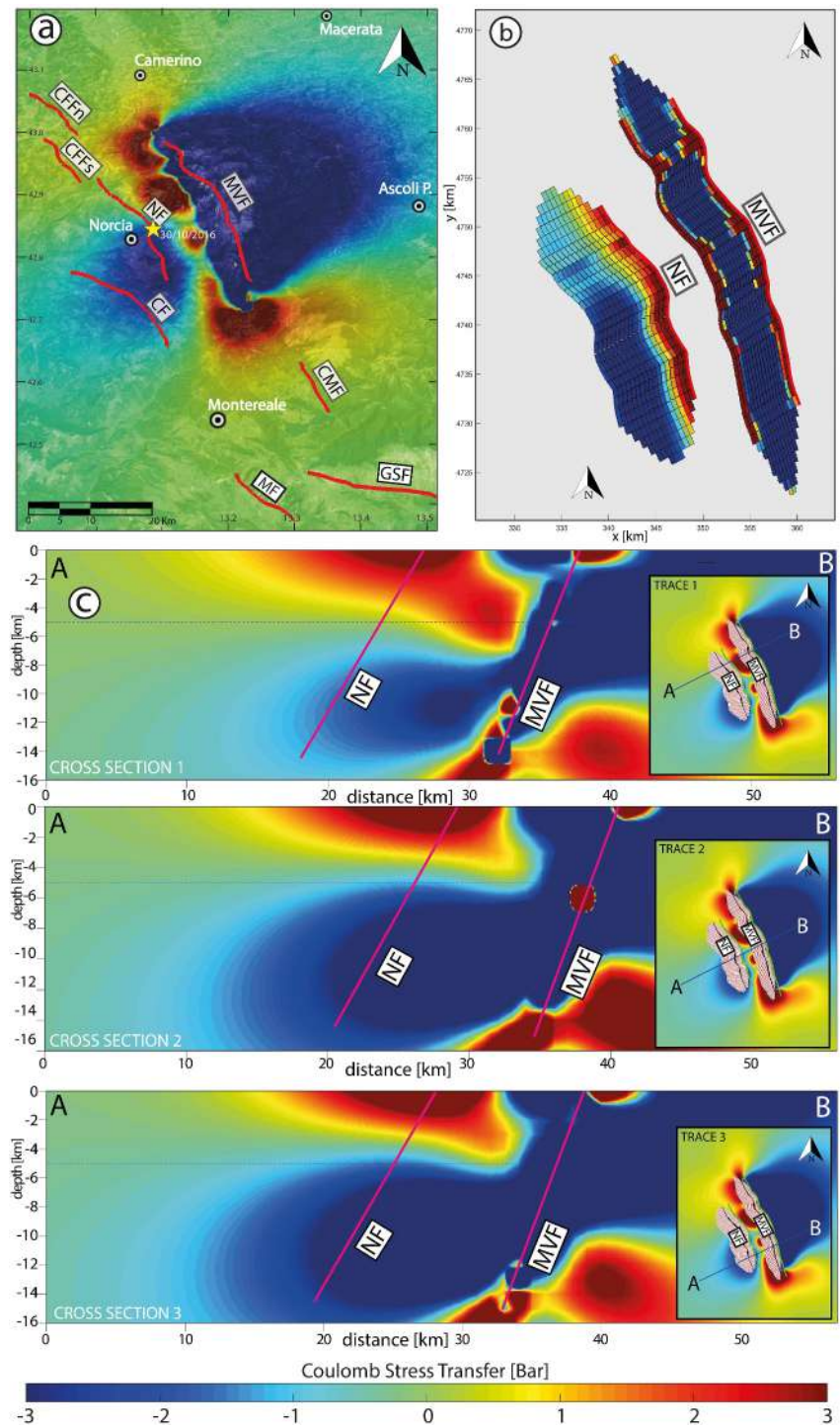


Figure 10. Coulomb stress transfer (CST) related to the 30 October 2016 earthquake. (a) Oblique view of the CST distribution on a plane located at a depth of 5 km. The causative fault is the Mt. Vettore Fault and the receiver is the Norcia fault. (b) 3D view of the CST on the causative and receiver faults. Note that the CST is calculated on each of the rectangles that make up the entirety of the fault. (c) Three cross-sections perpendicular to the Norcia fault placed in different portions along the receiver fault.

diminution particularly impacting the faults of Norcia (primarily its southern half) and Cascia. This stress shadow extends over 60 km eastward on the footwall. The plan view modeling (Figure 10a) at a depth of 5 km delineates four predominant lobes of increased stress, which are strategically positioned along the fault strike, confined to

the hanging wall and the northern and southern fault tips. The most expansive stress augmentation zone emanates from the southern tip of the Monte Vettore fault, progressing southward and imparting a minor CST (approximately 0.5 bars) exclusively to the northern segment of the Campotosto fault. Positive CST is also evident in the northern sector, affecting the Colfiorito faults and the northern half of the Norcia fault. Nonetheless, upon scrutinizing the three cross sections depicted in Figure 10c, it becomes evident that the Norcia fault (acting as the receiver fault in this simulation) undergoes a stress increase of up to 4 bars only within its shallower portion, spanning from approximately 4 km depth to the surface. This observation aligns with the conclusions of Galli et al. (2018) and Galderisi and Galli (2020), providing a rationale for the observed shallow coseismic ruptures on the Norcia fault due to the noted rise in surface stress. The fault's deeper segment is predominantly under the influence of the stress shadow, with negative values plummeting to around -4 bars. This distinct CST distribution along the Norcia fault is conspicuously discerned in the three-dimensional modeling (Figure 10b). This representation further elucidates that both the stress shadow and the stress rising zones display diminishing values as one transitions northward along the fault, consistent with the insights gleaned from the plan view.

4.8. Cumulative CST After 1997, 2009, and 2016 Earthquakes

The final model we considered seeks to elucidate the cumulative CST effect arising from seismic events spanning from 1997 to 2016. The objective behind this attempt is to understand the current stress state of the faults within the CAFS. For the plan view of this model, we utilized parameters from a hypothetical receiver fault, adopting average values of strike, dip, and rake representative of all the faults in the CAFS. This approach facilitated a broader applicability, enabling a more realistic assessment of the effects across the entire CAFS fault system. Noteworthy is the fact that multiple tests using varied receiver fault parameters were executed, yielding strikingly similar outcomes. This consistency is primarily attributed to the closely aligned range of dip, rake, and strike values among the CAFS faults, which rendered the differences in individual test outcomes nearly indiscernible.

Initial analysis of the resulting plan view model (Figure 11b) reveals complex interactions between the positive and negative stress lobes generated by different earthquakes. These lobes overlap, merge, and in some instances, cancel each other out or amplify each other. The resulting CST pattern is noticeably heterogeneous, characterized by dominant stress shadows interspersed with more localized regions of enhanced crustal stress. Delving deeper into the model at a depth of 5 km, we observed that the positive stress lobe, originating from the Mt Vettore fault activation and partially overlaying the Colfiorito fault, becomes obscured when juxtaposed with the pattern from the 1997 Colfiorito fault activation. Conversely, the positive stress lobe extending southeast from the Colfiorito fault is accentuated, intensifying the stress upon the Monte Vettore fault activation. This implies a pronounced cumulative positive stress state on the Norcia fault, especially its northern segment, which sits at the intersection of these positive CST lobes. The southern segment of the Norcia fault, however, remains predominantly in the stress shadow cast by the Monte Vettore fault, akin to the entirety of the Cascia fault.

Shifting further south reveals a compelling interplay between the positive stress lobes emanating from the 2016 Monte Vettore fault (propagating south from its southern fault tip) and the 2009 Paganica-San Demetrio fault (extending north from its northern tip). Their convergence forges a broad region of elevated stress around the area spanning from Montereale city to the Campotosto fault, subjecting the latter to an increased stress of approximately 1.2 bars. Both the Pettino and Marine faults are also enveloped by this heightened stress zone, a manifestation of the compounded cumulative stress effects triggered by nearby fault activations within a relatively short time frame.

In the plan view modeling at a depth of 5 km, the Gran Sasso fault appears to be influenced by a vast stress shadow created on the footwall of the Paganica-San Demetrio fault, which activated in 2009. However, this stress shadow covers the central area of the Gran Sasso fault, leaving the northernmost fault tip positively stressed. Greater complexity is revealed by the analysis of the three-dimensional model described below.

While the plan view was shaped by the hypothetical receiver fault and provides a general perspective of potential CST patterns from recent seismic events, a more granular model was constructed to depict the CST effect on every individual rectangular segment of each fault. Instead of relying on the hypothetical receiver fault parameters, this detailed model was tailored according to the specific strike, dip, and rake values of each discretized fault segment, yielding a notably refined result for each fault (Figure 11a). This representation unveils pronounced variations from the plan view. Key insights include the upper 5 km of the Norcia fault being predominantly affected by positive CST, with the northernmost section displaying stress penetration down to about 7 km. The superficial

layer of the fault experiences considerable stress intensities of up to 5 bars. Below these depths, the fault lies predominantly in the stress shadow engendered by the 1997 and 2016 earthquakes. The Cascia fault mirrors this pattern, with its topmost 2–3 km undergoing about 3.5 bars of positive stress while the underlying surface is primarily in the stress shadow. The Campotosto fault, in contrast, exhibits a more uniform positive stress profile, averaging around 0.8 bars.

The Mt Marine fault exhibits more heterogeneity in stress reception. Its southernmost fault tip experiences the highest CST, approximately 1.5 bars, which gradually decreases northward to around 0.5 bars. In contrast, the Pettino fault is primarily stressed at its northern tip and central region (up to about 1.2 bars), with the southern half influenced by the stress shadow caused by the 2009 Paganica-San Demetrio fault activation.

The Gran Sasso fault also displays intriguing CST dynamics. Its central and northern segments, extending to a depth of about 8 km, fall under the stress shadow produced by the Paganica-San Demetrio fault. Below this stress shadow and at the northern fault tip, the fault appears to experience positive CST up to a maximum of 2 bars. However, this stress concentration is confined to specific limited areas, leaving the southern half largely uninfluenced except for a slight stress reduction from the prominent bend toward the south, and this only at the surface. The stress accumulation at the extreme northern tip of the Gran Sasso fault does not exceed 0.7 bars.

5. Discussion

Our investigation into the dynamics of static stress transfer (CST) offers a comprehensive analysis of the CAFS, covering several centuries of $M_w \geq 6$ seismic events, from 1279 to 2016. This extensive temporal span allows a reliable understanding of the seismogenic sources behavior, capturing both the individual and cumulative CST effects of multiple seismic episodes and their implications for the current stress conditions within the CAFS.

The distribution of CST across the CAFS, characterized by concentrated areas of positive stress in some faults and shadow stress regions prevalent in others, underscores the complexity of seismic behavior within an interconnected fault system. The analyzed case studies have confirmed the role played by CST in adjacent faults, both in terms of earthquake triggering or inhibition. However, there are instances where this correlation is not so evident. The 1279 earthquake on the Colfiorito faults produced a zone of positive stress on the Norcia fault, that subsequently ruptured in 1328. Yet, the area of the Norcia fault affected by a considerable amount of stress is minimal and confined almost exclusively to its northern tip (Campi fault in Galli et al. (2023)). This finding let to speculate that the 1328 earthquake on the Norcia fault nucleated in the area of increased stress caused by the previous Colfiorito earthquake, to then engage the entire Norcia fault going southward. If so, the reactivation of the Norcia faults in 1328 might have been influenced by approximately 2 bars of positive stress at its northern extremity. As indicated by Galli et al. (2005) and Galderisi and Galli (2020), the 1328 earthquake did not involve the Cascia faults, as sometimes occurs in interconnected fault systems, but remained confined on the Norcia segments. In other words, the Cascia faults did not receive enough stress from the Colfiorito earthquake, supporting the hypothesis of stress transfer exclusively on the Norcia faults. A comparable situation is observed in simulations performed on the subsequent devastating 14 January 1703, Norcia earthquake. In this case, the entire Norcia fault system, including the Cascia faults, activated, producing a much energetic earthquake than in 1279 in Colfiorito. In 1703, the positive stress lobes reached much greater distances and higher values (bar), significantly affecting the northern segment of the Upper Aterno fault system, that is, the Mt Marine fault. Indeed, 19 days later, in the whole upper Aterno basin, a second devastating earthquake occurred, generated by the contemporary rupture of the Mt Marine, Mt Pettino and Paganica-San Demetrio fault, as also supported by the paleoseismological studies in Galli et al. (2010, 2011) and Moro et al. (2013). Despite the Paganica-San Demetrio fault was not affected by the CST generated by the January 1703 Norcia earthquake, the Mt Marine fault received enough stress to produce a cascade effect nucleating from this fault and then propagated southwards, involving, through dynamic and static stress transfer, also the other faults of the Upper Aterno fault system, in quick succession. Again, the influence of CST appears decisive.

However, it is worth noting that two and a half centuries earlier, the Gran Sasso fault system, running in the footwall of these faults, produced the most powerful earthquake in the CAFS. This $M_w \sim 7.0$ event put the UAFS, and in particular the upper part of the PSDFS into a situation of increasing stress. Even though much of the PSDFS was covered by the shadow zone of this large earthquake, it may have undergone dynamic stress transfer produced by the activation of the UAFS, which, on the contrary, were immersed in a substantial area of positive stress.

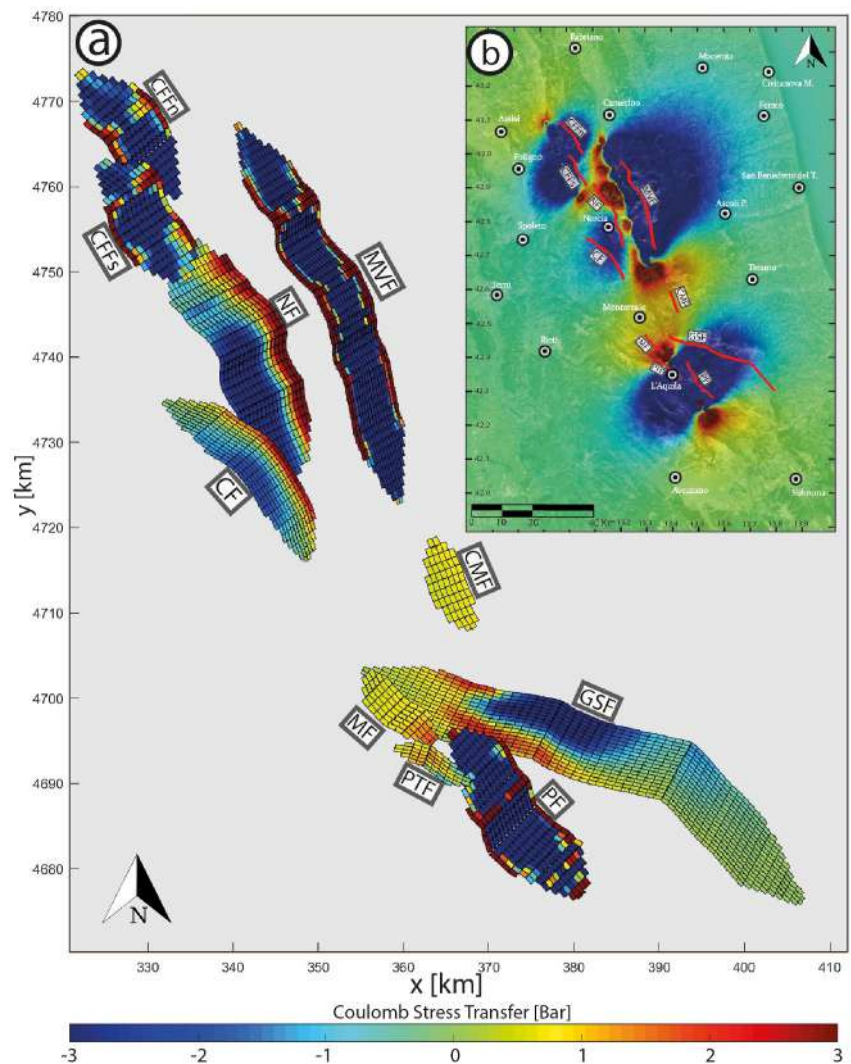


Figure 11. (a) 3D view of the cumulative Coulomb stress transfer (CST) in the CAFS following the 1997, 2009 and 2016 seismic sequences. Note that the CST is calculated on each of the small rectangles that make up the entirety of the faults. (b) Cumulative CST distribution at a depth of 5 km (plan view) following the 1997, 2009, and 2016 seismic sequences.

The 1703 Norcia earthquake also seems to have impacted the Campotosto fault, already in a critical situation in terms of CST from the 1349 Gran Sasso earthquake. Additionally, from the cumulative modeling of CST generated by recent instrumental earthquakes (Figures 11 and 13f), a significant positive stress contribution from recent earthquakes emerges. According to our models and calculations, the Campotosto fault would have reached a stress accumulation over a millennium that makes its lack of reactivation highly unlikely (Figures 12 and 13). Accordingly, the Campotosto fault has generated few seismic events with magnitudes just above Mw 5.0, both following the 2009 seismic sequence in L'Aquila and after the 2016 Mt. Vettore events (Cheloni et al., 2019; Galli, Galderisi, et al., 2022). This observation supports the hypothesis of Tondi et al. (2020), who consider the Campotosto fault to be an actual zone of soft-linkage between the northern and southern faults of the CAFS, deeming it a direct participant in recent seismic events.

Another cryptic situation concerns the activation of the Norcia fault in 1730 (Mw 6.0) following its earlier activation in 1703 (Mw 6.9). As this fault surely ruptured in 1703, the 1730 occurrence seems to challenge the theory that stress on the causative fault reduces to zero following its rupture. In order to generate another moderate magnitude earthquake only 27 years later, the fault would have needed to accumulate a significant amount of stress from neighboring faults, which really did not happen from 1703 to 1730. A possible explanation could be provided by Cowie et al. (2013), who demonstrated that in central Apennines nonlinear viscous deformation

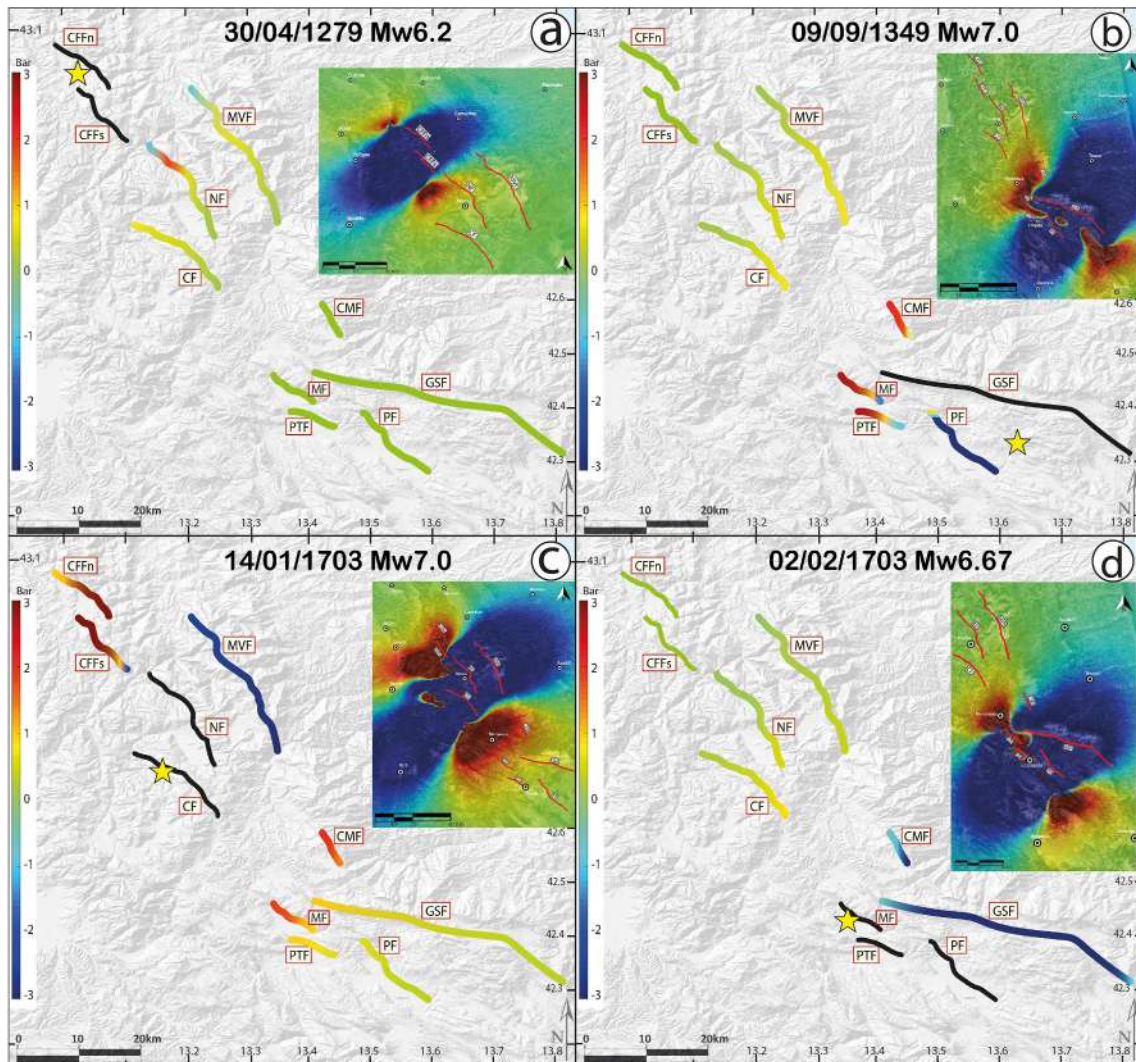


Figure 12. Summary visualization of the Calculated Coulomb stress transfer (CST) at a Depth of 5 km among the faults of the CAFS for each of the analyzed historical earthquakes. (a) CST generated by the Colfiorito Fault System in April 1279. (b) CST generated by the Gran Sasso Fault in September 1349. (c) CST generated by the Norcia and Cascia Faults in January 1703. (d) CST generated by the Paganica-San Demetrio fault, Marine, and Pettino Faults in February 1703. The fault traces drawn in black represent the causative faults. The insets of each figure illustrate the spatial distribution of the CST within the crust on a plane located at a depth of 5 km.

between 15 and 24 km depth dominates and promotes strain localization. Subsequently, Wedmore et al. (2017) calculated the interseismic loading of faults through continuous creep in shear zones at the base of each fault, below the locked brittle upper crust. Their study reveals that the Norcia fault, in the period between these two closely spaced earthquakes, managed to “recharge” with interseismic stress due to deep viscous deformation, partly aided by coseismic stress from smaller magnitude earthquakes that occurred earlier. This peculiarity could thus explain the close temporal reactivation of this fault within such a short time span.

In 1979, the Norcia fault generated an earthquake with a magnitude of Mw 5.83. This event was not considered in the CST calculations of this study, as its magnitude falls below the chosen threshold. However, it is worth noting that, given the position of the Colfiorito faults relative to the Norcia fault, this earthquake could have promoted stress to the Colfiorito fault system, facilitating its activation in 1997. It should also be mentioned that the faults responsible for the 1997 earthquake had already been subjected to considerable positive stress due to the devastating Norcia earthquake of 1703, further supporting the hypothesis that stress transfer played a crucial role.

In Figure 1, three closely located epicenters can be observed near the Cascia Fault (1599 Mw6.0, 1703 Mw6.9, and 1979 Mw5.83). The 1599 earthquake was caused by the Cascia Fault, followed by the 1703 Norcia fault

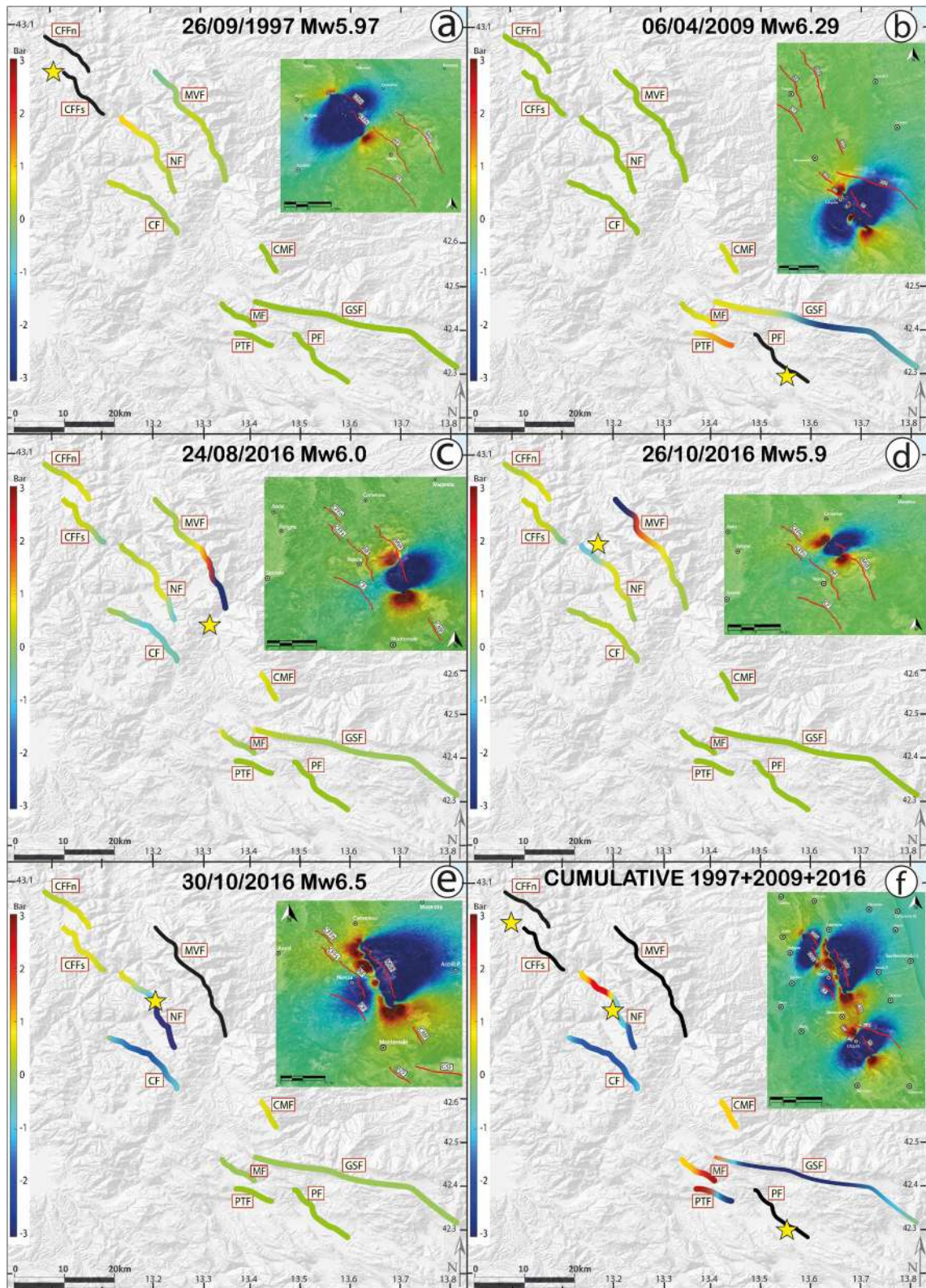


Figure 13.

system rupture, which reactivated the Cascia Fault. Finally, in 1979, only the Cascia Fault was involved. This fault ruptured three times within 180 years, suggesting that its stress did not drop to zero after the first two ruptures. It is plausible that the reactivation of the Cascia Fault in 1703, after 1599, was influenced by dynamic stress transfer caused by the major 1703 Norcia rupture (Mw 6.9), acting as a cascade effect. Between 1703 and 1979, two earthquakes occurred on the Norcia Fault (1730 and 1859), which, although of low-moderate magnitude, could have transferred enough positive stress to the Cascia Fault, facilitating its recent rupture.

While for historical earthquakes CST modeling may have been influenced by uncertainty regarding their real magnitude, CST calculations for recent earthquakes (1997 Colfiorito, 2009 L'Aquila, and 2016 Mt. Vettore earthquakes) are more reliable as slip data are available, and there is not error on the magnitude. This allowed us to model the slip on Mt. Vettore fault exactly as it occurred, divided into three main shocks that involved different portions of the fault.

In the case of Mt. Vettore, an unusual scenario is observed; the first partial activation predominantly impacted the southern tip, stressing the central region of the fault and sparing the northern tip. Nevertheless, the latter was the subsequent segment to activate. Historically, the northern segment has never been subjected to significant positive stress loading. However, Mildon et al. (2017) attributed this anomaly to the interseismic stress loading in the shear zone at 15–24 km depth, which would have positively stressed the deeper band of the fault. According to these authors, this would have predisposed the fault to a subsequent earthquake. After 24 August (Mw 6.0) event, on 26 October (Mw 5.9) the northern tip ruptured, significantly increasing stress in the fault's central region. However, on 30 October, not only the central portion of the fault, but also the previously ruptured segments reactivated, indicating that the accumulated stress had not fully dissipated. The previous coseismic rupture of the Mt. Vettore fault occurred 1573 years earlier (Galli, Galderisi, Marinelli, et al., 2019; Galli, Galderisi, Peronace, et al., 2019), and the recurrence interval for an earthquake of similar magnitude is approximately 1.8 ± 0.3 Kyr, suggesting a slightly advanced recurrence time for the Mt. Vettore fault. Interestingly, the 1703 Norcia earthquake simulation reveals that the Mt. Vettore fault experienced significant negative inhibiting stress, with no other models displaying sufficient positive CST to compensate for the stress removed in 1703. Different mechanisms such as fluid migration, dynamic stress transfer or interseismic stress loading may be invoked in this situation (Brodsky & van der Elst, 2014; Hetzel & Hampel, 2005; Oskin et al., 2008; Wedmore et al., 2017).

The CST pattern generated in 2016 on the Norcia Fault aligns with the calculations made by Galderisi and Galli (2020), corroborating the theory that these two faults exchange CST in a mutually inhibitory manner. Moreover, our calculations indicate that the Norcia fault experiences significantly higher stress up to a depth of approximately 5 km, this data supports the findings of these authors, justifying the superficial coseismic ruptures on the Norcia fault with the aforementioned increase in surface stress.

The case study of the earthquake that struck the L'Aquila area in 2009 has revealed interesting implications for stress transfer to the Gran Sasso fault. Valoroso et al. (2013) conducted a thorough crustal study following this seismic event to analyze the distribution of aftershocks and deduce the geometry of the fault system. This detailed distribution of hypocenters suggests that some of them fall on the northern sector of the Gran Sasso fault. Galli, Galderisi, et al. (2022) analyzed the distribution of these aftershocks in comparison with the two northern segments of the Gran Sasso fault, finding a precise correlation, with two aftershock clusters appearing to coincide perfectly with these fault segments. In particular, it seems that three significant aftershocks (Mw 4.0, Mw 4.7, Mw 5.1) are due to the reactivation of this major fault system. Our CST model in Figure 11 highlights the stress state of the Gran Sasso fault following recent seismic events. It can be stated that the stress pattern evident on the Gran Sasso fault is almost exclusively due to the 2009 L'Aquila earthquake, thus it is noticeable how the central deep and northern portions have been subjected to a significant increase in stress following the 2009 earthquake. The distribution of the L'Aquila earthquake aftershocks seems to coincide with the positively stressed areas of the GSF, corroborating the hypothesis of Galli, Galderisi, et al. (2022). Indeed, we can observe how the two faults (PSDF and GSF), having different strikes, tend to converge toward their northwestern tips, making the stress

Figure 13. Summary visualization of the Calculated Coulomb stress transfer (CST) at a depth of 5 km among the faults of the CAFS for each of the analyzed instrumental earthquakes. (a) CST generated by the Colfiorito Fault System in September 1997. (b) CST generated by the Paganica-San Demetrio Fault in April 2009. (c) CST generated by the southern portion of the Mt. Vettore fault in August 2016. (d) CST generated by the northern portion of the Mt. Vettore fault on 26 October 2016. (e) CST generated by the complete rupture of the Mt. Vettore fault on 30 October 2016. (f) Cumulative CST from the last five instrumental earthquakes. The fault traces drawn in black represent the causative faults. The insets of each figure illustrate the spatial distribution of the CST within the crust on a plane located at a depth of 5 km.

transfer more effective in the northwest sector of the Gran Sasso fault compared to the southern half, which seems only partially influenced. The positive correlation between the stress pattern and the distribution of aftershocks provides further confirmation of the ability of CST to guide the evolution of seismic sequences. The 2009 earthquake, caused by the Paganica-San Demetrio fault, occurred in a fault that accumulated significant negative static stress from the 1349 Gran Sasso earthquake. Only the shallow portion of the Paganica-San Demetrio Fault received positive stress, contributing to two other subsequent earthquakes. Assuming stress on a fault drops to zero after a seismic event (and Paganica-San Demetrio Fault caused two before 2009), we can exclude the influence of the 1349 and 1461 earthquakes on the 2009 fault rupture.

Beyond the boundaries of the CAFS, two historically seismically-active regions to the north and south, Fabriano and Sulmona, respectively, have remained dormant in recent centuries (Bordoni et al., 2023; Castelli & Monachesi, 2001; Galli et al., 2015; Gironelli et al., 2023; Gori et al., 2011; Stucchi et al., 1991). The following are estimates, as we do not know the exact position and kinematics of the Fabriano fault, making precise CST calculations impossible. Additionally, the Fabriano and Sulmona faults lie outside the CAFS; therefore, we did not include them in our calculations and did not incorporate the earthquakes they generated into our data. The stress pattern shown in Figure 11b refers to a receiver fault with kinematics and orientation corresponding to an average of those belonging to the CAFS. If the Fabriano fault significantly deviates from the orientation and kinematics of the CAFS faults, the result would be different. Despite this, interactions between the CAFS activity and the Fabriano and Sulmona faults can be hypothesized given their proximity and similar seismotectonic context. Below, we will make considerations about these two zones north and south of the CAFS, taking into account the uncertainty due to the lack of specific calculations but based on the extent of the stressed zones from historical and instrumental earthquakes of the CAFS. We are prepared to perform specific calculations should new scientific information emerge about the earthquake that struck the city of Fabriano in 1741. Our model suggests that these areas are minimally impacted by recent seismic sequences, recording only negligible stress changes (up to a maximum of 0.3 bars) (Figure 11b). Nevertheless, historical events amplify concerns. For example, the 1349 earthquake on the Gran Sasso fault transferred modest amounts of stress to the Mt Morrone fault, which borders the Sulmona basin. This calculation can be considered more precise compared to that of Fabriano because the Mt. Morrone fault, near Sulmona, has an orientation and kinematics similar to those of the CAFS. Moving north, the 1703 Norcia earthquake imparted positive stress to the crust surrounding Fabriano. Although the seismogenic source of the Fabriano earthquake is still debated in literature (Basili et al., 2008; Cello et al., 1997; Gironelli et al., 2023; Materazzi et al., 2022 and references therein), it triggered a significant Mw 6.1 earthquake in 1741, a few decades after the Norcia earthquake, suggesting probable stress transfer influence. In contrast, the Mt Morrone fault has not generated significant earthquakes for over 1800 years (Galli et al., 2015), heightening concern regarding this significant fault.

Examining the differences in seismic moment release across the three seismicity windows described by Valentini et al. (2023), further insights can be drawn. The authors characterize the seismic cycle of the CAFS over the past millennium as segmented into three periods of higher seismicity, each registering a distinct cumulative seismic moment. Assuming that a millennium is a sufficiently long period to characterize the seismic cycle of the CAFS, one can make considerations on its predictability and a possible recurrence model. Several authors have demonstrated that many fault systems exhibit a time-predictable nature (e.g., Rubinstein et al., 2012; Scholz, 2019; Shimazaki & Nakata, 1980; Zechar & Nadeau, 2012), while Tondi and Cello (2003) have suggested the time-and-slip-predictable nature of the CAFS. If we accept the latter assertion as correct and consider the significant difference in seismic moment (dependent on slip and thus directly proportional) between the first two seismicity windows (one between 1300 and 1400, one around 1700) and the most recent one (from 1979 to 2016), we can hypothesize the existence of a seismic moment gap in the current historical period. This hypothesis assumes the immutability of the displacement rate over such a short time frame, which over the last 700 ka is 1.6 cm/year (for the entire CAFS; Tondi & Cello, 2003). The lowest cumulative seismic moment is thus observed in the latest seismicity window, corresponding to the period from 1979 to 2016. Consequently, there appears to be a potential seismic gap in the current historical period, which, according to the authors calculations, could be filled with a seismic moment of approximately $M_0 = 1.27E + 26$ dyne-cm, corresponding to a magnitude $M_w = 6.67$ earthquake. Such magnitude might be generated by the Gran Sasso fault, which, as deduced from Figure 11a, exhibits zones of particularly high stress. Moreover, this fault has shown no signs of reactivation since 1349 and, despite often falling within the stress shadows of adjacent faults, displays a considerably long temporal gap of

inactivity. On the other hand, the Gran Sasso fault seems to be characterized by long recurrence times (2.8 ± 0.5 ky; Galli, Galderisi, et al., 2022), and although CST may influence the characteristic return time (e.g., Wedmore et al., 2017), it still remains an extremely lengthy period.

The CAFS could be spatially divided into two sectors, the northern sector encompassing the fault systems of Colfiorito, Mt Vettore and Norcia, and the southern sector those of the Upper Aterno, Laga Mts, and Gran Sasso. During the latest seismicity window, most of the seismic moment was generated by the northern sector, leaving the southern sector affected only by the southern segments of the UAFS, namely the Paganica-San Demetrio faults, which are insufficient to bridge the aforementioned seismic gap. This thesis supports the hypothesis that the causative fault for the seismic gap could belong to the southern sector.

Our study also highlights the cumulative nature of CST, with subsequent seismic events either amplifying or compensating for the stress effects of prior events. This iterative accumulation of stress alterations may result in stress conditions significantly different from those inferred from isolated events, emphasizing the importance of a comprehensive and long-term perspective on seismic sequences to understand their stress impacts. The importance of considering individual fault characteristics in CST modeling becomes evident from our analysis. While an aggregate model based on average fault parameters provides valuable insights into potential CST patterns, a detailed model designed for specific values of strike, dip, and rake for each fault segment offers a more refined understanding of the CST effects on each fault.

However, it is worth noting that the accuracy of our models depends on the precision of input parameters, which, although derived from the best available data, remain approximations. For example, so far, determining the slip patterns of historical earthquakes is impossible. Moreover, Vannucci et al. (2021) have pointed out that historical earthquakes might be overvalued in magnitude due to the challenges of estimating their size from macroseismic data. Such inaccuracies could result in overrating the energy released during pre-instrumental seismic events. Furthermore, calculated CST changes do not necessarily forecast an earthquake but merely indicate the stress state of a fault. This aligns with observations by Hardebeck et al. (1998), who noted that although CST models offer valuable insights, their predictive ability remains inherently probabilistic.

Our study underscores the crucial role of spatial and temporal components of CST in understanding seismic dynamics. It emphasizes the value of considering the cumulative effects of multiple seismic events and the specific characteristics of individual faults in seismic behavior modeling. Future studies may seek to further refine these models by incorporating more detailed fault characteristics and broader geographic contexts to improve the precision of seismic risk predictions.

6. Conclusions

The Central Apennines Fault System (CAFS) is an active tectonic region in central Italy which caused a series of devastating seismic events in the past Millennium. While the role of CST in triggering seismic events has been discussed in numerous studies, its specific influence within the CAFS over an extensive time span has remained analytically unexplored. This research addresses that gap by providing an in-depth analysis of the effects of CST on historical and instrumental seismic events associated with the CAFS.

Nine selected events from the CPTI15 catalog were tested for comprehensive CST analysis, based on their spatiotemporal proximity to subsequently activated faults. In addition, in order to isolate the static stress transfer for each seismic episode, we analyzed the cumulative CST of contemporary instrumental earthquakes, detailing the current stress landscape. Employing an innovative methodology, faults were conceptualized in a three-dimensional plane, with an ellipse-shaped area implying their 2D geometric representation. Given the sensitivity of CST to strike variations, a variable strike was integrated within a three-dimensional elliptical model, ensuring greater accuracy in estimates.

In many of the case studies, CST may have played an influential role within the CAFS, catalyzing the activation or inhibition of its faults. Several instances highlight fault reactivation following high stress transfer between closely outcropping active faults, in short periods. Some examples are described below:

- The 1279 Colfiorito earthquake positively stressed the northern tip of the Norcia fault, that actually ruptured few decades later, in 1328.

- The 14 January 1703, Norcia earthquake positively stressed the Mt. Marine fault, where few days later a huge earthquake nucleated, provoking a cascade effect engaging the whole Upper Aterno fault system, namely the Mt. Marine-Mt. Pettino-Paganica-San Demetrio faults.
- The August 24 and 26 October 2016, earthquakes seem to have stressed the bends and the central portion of the Mt. Vettore fault, probably facilitating the October 30 impressive surface fault rupture.
- The Colfiorito fault system stored conspicuous amount of positive stress from each of the earthquakes generated by the Norcia fault system, including the 1979 event (Mw 5.83), probably influencing its reactivation in 1997.
- The 14 January 1703, Norcia earthquake generated also a huge positive stress lobe toward the Fabriano area, where 38 years later a destructive earthquake struck.

Conversely, certain scenarios illuminate the calming effect of stress shadows. Some examples include:

- The Mt. Vettore fault generated only two earthquakes during the past two millennia. This could be linked to the existence of the parallel Norcia fault that ruptured at least 5 times in the same interval, transferring negative CST on the Vettore fault.
- The same hypothesis could be applied to the Gran Sasso fault, which ruptured only in 1349 in the past millennium, whereas the Upper Aterno and the Paganica-San Demetrio fault systems generated at least 3 strong earthquakes that transferred negative Coulomb stress on the Gran Sasso fault.

However, some events do not display a clear correlation, suggesting the influence of other factors, such as fluid dynamics, accumulated elastic strain energy, interseismic stress loading or dynamic stress transfer. Some examples of this lack of correlation are:

- The 1349 Gran Sasso earthquake enveloped the Paganica-San Demetrio fault in a huge stress shadow, but the latter ruptured 112 years later, in 1461.
- The February 1703 Upper Aterno earthquake exerted a negligible influence on the Norcia fault, but the latter ruptured 27 years later notwithstanding the huge stress drop on the fault during the previous January 1703 Norcia earthquake.
- The 1997 Colfiorito earthquake transferred a negligible amount of stress to the Mt. Vettore fault, and almost exclusively on its central portion, but the southernmost portion of the fault ruptured during the August 2016 earthquake.
- The CST caused by the 2009 Paganica-San Demetrio fault earthquake did not affect the Vettore fault that generated the 2016 earthquake.

The nuanced understanding of CST achieved through this research has both concrete and academic implications. By illuminating the interaction between faults in previous seismic episodes, it provides valuable insights into potential future earthquake sequences. Such awareness is essential: by anticipating seismic sequences, targeted risk mitigation tactics can be formulated, thereby protecting local communities from the catastrophic consequences of earthquakes.

Moreover, the complexity of the CAFS, observed in light of past seismic episodes like those in 1997, 2009, and 2016, underscores the intricate nature of stress patterns. These patterns emerge from interactions between seismic events, with stress lobes intertwining in ways that amplify, nullify, or diversify their impacts on nearby faults. It is noteworthy that while historically and currently seismic-active regions such as Fabriano and Sulmona have remained relatively quiescent, their potential for future activity and associated risks should not be overlooked. This research highlights the complex dynamics at play in a high-seismic-activity region like the CAFS. Through rigorous analyses and innovative modeling techniques, we offer insights that can guide future investigations and pragmatic strategies for seismic risk mitigation. This study stands as a testament to the profound ability of CST to influence the seismic narrative of a region and emphasizes the need for continued research in this field.

Data Availability Statement

For the creation of this manuscript, data were sourced from the Italian Catalogue of Active and Capable Faults (ITHACA- Italy Hazard from Capable faults; ITHACA Working Group, 2019; <http://sgi2.isprambiente.it/ithacaweb/Mappatura.aspx>) and the Database of Individual Seismogenic Sources (DISS; DISS Working Group, 2021; Basili et al., 2008; <https://diss.ingv.it>), comparing the data in these catalogs with those found in

scientific literature for each fault. Earthquake data were cross-referenced with various seismic catalogs, including the Parametric Catalogue of Italian Earthquakes (CPTI15; Rovida et al., 2022; <https://emidius.mi.ingv.it/CPTI15-DBMI15>), the Italian Seismological Instrumental and Parametric Data-Base (ISIDE; ISIDE Working Group, 2007; <https://terremoti.ingv.it/iside>), the Catalogue of Strong Italian Earthquakes (CFTI; Guidoboni et al., 2018, 2019; <https://storing.ingv.it/cfti/cfti5/>), and the Italian Macroseismic Database (DBMI; Locati et al., 2022; <https://emidius.mi.ingv.it/CPTI15-DBMI15>). Some finite-fault rupture models were derived from the Earthquake Source Model Database (SRCMOD; Mai & Thingbaijam, 2014; <http://equake-rc.info/srcmod>) and were used as input for specific Matlab (MATLAB Version: 9.14.0.2137306 (R2023a) Prerelease—academic license; The MathWorks Inc. (2022; <https://www.mathworks.com>)) tools. The Matlab tools employed are “Coulomb3.4” (Lin & Stein, 2004; Toda et al., 2005; <https://temblor.net/coulomb/>) and “Faults 3D” (Mildon, Toda, et al., 2016; <https://github.com/ZoeMildon/3D-faults>). Figures were created using Adobe Illustrator (version 28.3; Adobe Inc, 2019a), Adobe Photoshop (version 25.5; Adobe Inc, 2019b) and Google Earth Pro (<http://www.google.com/earth/index.html>).

Acknowledgments

We would like to acknowledge Dr. Zoë Mildon and Dr. Manuel-Lukas Diercks for their kind assistance in using the “3D-Faults” MATLAB code. This work was supported by the FAR Unicam project “Novel Approach for Seismic Hazard Analysis—NoHard,” responsible Emanuele Tondi. Open access publishing facilitated by Università degli Studi di Camerino, as part of the Wiley - CRUI-CARE agreement.

References

- Adobe Inc. (2019a). Adobe Illustrator. Retrieved from <https://adobe.com/products/illustrator>
- Adobe Inc. (2019b). Adobe Photoshop. Retrieved from <https://www.adobe.com/products/photoshop.html>
- Aki, K., & Richards, P. G. (1980). In J. Ellis (Ed.), *Quantitative seismology* (2nd ed.). University Science Books.
- Alkan, H., Öztürk, S., & Akkaya, İ. (2023). Seismic hazard implications in and around the Yedisu Seismic Gap (Eastern Türkiye) based on Coulomb stress changes, *b*-values, and *S*-wave velocity. *Pure and Applied Geophysics*, 180(9), 3227–3248. <https://doi.org/10.1007/s00024-023-03342-7>
- Amato, A., Azzara, R., Chiarabba, C., Cimini, G. B., Cocco, M., Di Bona, M., et al. (1998). The 1997 Umbria-Marche, Italy, earthquake sequence: A first look at the main shocks and aftershocks. *Geophysical Research Letters*, 25(15), 2861–2864. <https://doi.org/10.1029/98gl51842>
- Anderson, E. M. (1951). *The dynamics of faulting*. Oliver & Boyd.
- Anzidei, M., Boschi, E., Cannelli, V., Devoti, R., Esposito, A., Galvani, A., et al. (2009). Coseismic deformation of the destructive April 6, 2009, L'Aquila earthquake (central Italy) from GPS data. *Geophysical Research Letters*, 36(17), L17307. <https://doi.org/10.1029/2009gl039145>
- Asayesh, B. M., Zafarani, H., & Tatar, M. (2020). Coulomb stress changes and secondary stress triggering during the 2003 (Mw 6.6) Bam (Iran) earthquake. *Tectonophysics*, 775, 228304. <https://doi.org/10.1016/j.tecto.2019.228304>
- Barchi, M., Galadini, F., Lavecchia, G., Messina, P., Michetti, A. M., Peruzza, L., et al. (2000). *Sintesi delle conoscenze sulle faglie attive in Italia Centrale: Parametizzazione ai fini della caratterizzazione della pericolosità sismica*. GNDT-Monografie.
- Basili, R., Valensise, G., Vannoli, P., Burrato, P., Fracassi, U., Mariano, S., & Boschi, E. (2008). The database of individual seismogenic sources (DISS), version 3: Summarizing 20 years of research on Italy's earthquake geology. *Tectonophysics*, 453(1–4), 20–43. <https://doi.org/10.1016/j.tecto.2007.04.014>
- Blumetti, A. M. (1995). Neotectonic investigation of evidence of paleoseismicity in the epicentral area of the January–February 1703, central Italy, earthquakes. In L. Serva (Ed.), *Perspectives in Paleoseismology* (Vol. 6, pp. 83–100). Bulletin of the American Association of Engineering Geologists.
- Boncio, P., & Lavecchia, G. (2000). A structural model for active extension in Central Italy. *Journal of Geodynamics*, 29(3–5), 233–244. [https://doi.org/10.1016/s0264-3707\(99\)00050-2](https://doi.org/10.1016/s0264-3707(99)00050-2)
- Boncio, P., Lavecchia, G., & Pace, B. (2004). Defining a model of 3D seismogenic sources for Seismic Hazard Assessment applications: The case of central Apennines (Italy). *Journal of Seismology*, 8(3), 407–425. <https://doi.org/10.1023/b:jose.0000038449.78801.05>
- Bordoni, P., Gori, S., Akinci, A., Visini, F., Sgobba, S., Pacor, F., et al. (2023). A site-specific earthquake ground response analysis using a fault-based approach and nonlinear modeling: The Case Pente site (Sulmona, Italy). *Engineering Geology*, 314, 106970. <https://doi.org/10.1016/j.enggeo.2022.106970>
- Brodsky, E. E., & van der Elst, N. J. (2014). The uses of dynamic earthquake triggering. *Annual Review of Earth and Planetary Sciences*, 42(1), 317–339. <https://doi.org/10.1146/annurev-earth-060313-054648>
- Byerlee, J. (1978). Friction of rocks. *Pure and Applied Geophysics*, 116, 615–626. https://doi.org/10.1007/978-3-0348-7182-2_4
- Camassi, R., Galli, P., Molin, D., Monachesi, G., & Morelli, G. (1997). Rilievo macrosismico preliminare del terremoto umbro-marchigiano di settembre-ottobre 1997. *Ingegneria Sismica*, 4, 50–54.
- Castelli, V., & Monachesi, G. (2001). Seismic history and historical earthquake scenario for the town of Fabriano (Central Italy). *Italian Geotechnical Journal*, 35(2), 36–46.
- Cello, G., Deiana, G., Mangano, P., Mazzoli, S., Tondi, E., Ferrelli, L., et al. (1998). Evidence for surface faulting during the September 26, 1997, Colfiorito (Central Italy) earthquakes. *Journal of Earthquake Engineering*, 2(2), 303–324. <https://doi.org/10.1080/13632469809350324>
- Cello, G., Mazzoli, S., Tondi, E., & Turco, E. (1995). Tettonica attiva in Appennino centrale ed implicazioni per l'analisi della pericolosità sismica del settore assiale della catena umbro-marchigiana-abruzzese. *Studi Geologici Camerti. Nuova Serie*, 13(1), 115–138.
- Cello, G., Mazzoli, S., Tondi, E., & Turco, E. (1997). Active tectonics in the central Apennines and possible implications for seismic hazard analysis in peninsular Italy. *Tectonophysics*, 272(1), 43–68. [https://doi.org/10.1016/S0040-1951\(96\)00275-2](https://doi.org/10.1016/S0040-1951(96)00275-2)
- Cheloni, D., D'Agostino, N., Scognamiglio, L., Tinti, E., Bignami, C., Avallone, A., et al. (2019). Heterogeneous behavior of the Campotosto normal fault (Central Italy) imaged by InSAR GPS and strong-motion data: Insights from the 18 January 2017 events. *Remote Sensing*, 11(12), 1482. <https://doi.org/10.3390/rs11121482>
- Chiarabba, C., Amato, A., Anselmi, M., Baccheschi, P., Bianchi, I., Cattaneo, M., et al. (2009). The 2009 L'Aquila (central Italy) M_w 6.3 earthquake: Main shock and aftershocks. *Geophysical Research Letters*, 36(18), L18308. <https://doi.org/10.1029/2009gl039627>
- Chiarabba, C., & De Gori, P. (2016). The seismogenic thickness in Italy: Constraints on potential magnitude and seismic hazard. *Terra Nova*, 28(6), 402–408. <https://doi.org/10.1111/ter.12233>
- Chiaraluce, L. (2012). Unravelling the complexity of Apenninic extensional fault systems: A review of the 2009 L'Aquila earthquake (Central Apennines, Italy). *Journal of Structural Geology*, 42, 2–18. <https://doi.org/10.1016/j.jsg.2012.06.007>

- Chiaraluce, L., Valoroso, L., Piccinini, D., Di Stefano, R., & De Gori, P. (2011). The anatomy of the 2009 L'Aquila normal fault system (central Italy) imaged by high resolution foreshock and aftershock locations. *Journal of Geophysical Research*, *116*(B12), B12311. <https://doi.org/10.1029/2011jb008352>
- Cinti, F. R., Pantosti, D., De Martini, P. M., Pucci, S., Civico, R., Pierdominici, S., et al. (2011). Evidence for surface faulting events along the Paganica fault prior to the 6 April 2009 L'Aquila earthquake (central Italy). *Journal of Geophysical Research*, *116*(B7), B07308. <https://doi.org/10.1029/2010jb007988>
- Collettini, C., & Sibson, R. H. (2001). Normal faults, normal friction? *Geology*, *29*(10), 927–930. [https://doi.org/10.1130/0091-7613\(2001\)029<0927:nfnf>2.0.co;2](https://doi.org/10.1130/0091-7613(2001)029<0927:nfnf>2.0.co;2)
- Cowie, P. A., Scholz, C. H., Roberts, G. P., Faure Walker, J. P., & Steer, P. (2013). Viscous roots of active seismogenic faults revealed by geologic slip rate variations. *Nature Geoscience*, *6*(12), 1036–1040. <https://doi.org/10.1038/ngeo1991>
- DISS Working Group. (2021). *Database of Individual Seismogenic Sources (DISS), version 3.3.0: A compilation of potential sources for earthquakes larger than M 5.5 in Italy and surrounding areas*. Istituto Nazionale di Geofisica e Vulcanologia (INGV). <https://doi.org/10.13127/diss3.3.0>
- Dong, P., Zhao, B., & Qiao, X. (2022). Interaction between historical earthquakes and the 2021 Mw7.4 Maduo event and their impacts on the seismic gap areas along the East Kunlun fault. *Earth Planets and Space*, *74*(1), 42. <https://doi.org/10.1186/s40623-022-01589-3>
- EMERGEIO Working Group. (2010). Evidence for surface rupture associated with the Mw 6.3 L'Aquila earthquake sequence of April 2009 (central Italy). *Terra Nova*, *22*(1), 43–51. <https://doi.org/10.1111/j.1365-3121.2009.00915.x>
- Faluccci, E., Gori, S., Moro, M., Fubelli, G., Saroli, M., Chiarabba, C., & Galadini, F. (2015). Deep reaching versus vertically restricted Quaternary normal faults: Implications on seismic potential assessment in tectonically active regions: Lessons from the middle Aterno valley fault system, central Italy. *Tectonophysics*, *651*, 186–198. <https://doi.org/10.1016/j.tecto.2015.03.021>
- Faure Walker, J. F., Roberts, G. P., Cowie, P. A., Papanikolaou, I., Michetti, A. M., Sammonds, P., et al. (2012). Relationship between topography, rates of extension and mantle dynamics in the actively-extending Italian Apennines. *Earth and Planetary Science Letters*, *325*, 76–84. <https://doi.org/10.1016/j.epsl.2012.01.028>
- Faure Walker, J. P., Roberts, G. P., Cowie, P. A., Papanikolaou, I. D., Sammonds, P. R., Michetti, A. M., & Phillips, R. J. (2009). Horizontal strain-rates and throw-rates across breached relay zones, central Italy: Implications for the preservation of throw deficits at points of normal fault linkage. *Journal of Structural Geology*, *31*(10), 1145–1160. <https://doi.org/10.1016/j.jsg.2009.06.011>
- Faure Walker, J. P., Roberts, G. P., Sammonds, P. R., & Cowie, P. (2010). Comparison of earthquake strains over 102 and 104 year timescales: Insights into variability in the seismic cycle in the central Apennines, Italy. *Journal of Geophysical Research*, *115*(B10), B10418. <https://doi.org/10.1029/2009JB006462>
- Fossen, H. (2016). *Structural geology*. Cambridge University Press.
- Galadini, F., & Galli, P. (2000). Active tectonics in the central Apennines (Italy)—input data for seismic hazard assessment. *Natural Hazards*, *22*(3), 225–268. <https://doi.org/10.1023/a:1008149531980>
- Galadini, F., & Galli, P. (2003). Paleoseismology of silent faults in the Central Apennines (Italy): The Mt. Vettore and Laga Mts. faults. *Annales Geophysicae*, *465*, 815–836.
- Galadini, F., & Messina, P. (2001). Plio-Quaternary changes of the normal fault architecture in the central Apennines (Italy). *Geodinamica Acta*, *14*(6), 321–344. [https://doi.org/10.1016/s0985-3111\(01\)01076-2](https://doi.org/10.1016/s0985-3111(01)01076-2)
- Galderisi, A., & Galli, P. (2020). Coulomb stress transfer between parallel faults. The case of Norcia and Mt Vettore normal faults (Italy, 2016 Mw 6.6 earthquake). *Results in Geophysical Sciences*, *1–4*, 100003. <https://doi.org/10.1016/j.ringsp.2020.100003>
- Galli, P., Camassi, R., Azzaro, R., Bernardini, F., Castenetto, S., Molin, D., et al. (2009). Il terremoto aquilano del 6 aprile 2009: Rilievo macrosismico, effetti di superficie ed implicazioni sismotettoniche. *Alpine and Mediterranean Quaternary*, *22*(2), 235–246.
- Galli, P., & Galadini, F. (1999). Seismotectonic framework of the 1997–98 Umbria-Marche (Central Italy) earthquakes. *Seismological Research Letters*, *70*(4), 404–414.
- Galli, P., Galadini, F., & Calzoni, F. (2005). Surface faulting in Norcia (central Italy): A “paleoseismological perspective”. *Tectonophysics*, *403*(1–4), 117–130. <https://doi.org/10.1016/j.tecto.2005.04.003>
- Galli, P., Galadini, F., & Pantosti, D. (2008). Twenty years of paleoseismology in Italy. *Earth-Science Reviews*, *88*(1–2), 89–117. <https://doi.org/10.1016/j.earscirev.2008.01.001>
- Galli, P., Galderisi, A., Ilardo, I., Piscitelli, S., Scionti, V., Bellanova, J., & Calzoni, F. (2018). Holocene paleoseismology of the Norcia fault system (Central Italy). *Tectonophysics*, *745*, 154–169. <https://doi.org/10.1016/j.tecto.2018.08.008>
- Galli, P., Galderisi, A., Marinelli, R., Peronace, E., Messina, P., & Polpetta, F. (2019). A reappraisal of the 1599 earthquake in Cascia (Italian Central Apennines): Hypothesis on the seismogenic source. *Tectonophysics*, *774*, 228287. <https://doi.org/10.1016/j.tecto.2019.228287>
- Galli, P., Galderisi, A., Messina, P., & Peronace, E. (2022). The Gran Sasso fault system: Paleoseismological constraints on the catastrophic 1349 earthquake in Central Italy. *Tectonophysics*, *822*, 229156. <https://doi.org/10.1016/j.tecto.2021.229156>
- Galli, P., Galderisi, A., Peronace, E., Giaccio, B., Hajdas, I., Messina, P., et al. (2019). The awakening of the dormant Mount Vettore fault (2016 central Italy earthquake, Mw 6.6): Paleoseismic clues on its millennial silences. *Tectonics*, *38*(2), 687–705. <https://doi.org/10.1029/2018tc005326>
- Galli, P., Giaccio, B., & Messina, P. (2010). The 2009 central Italy earthquake seen through 0.5 Myr-long tectonic history of the L'Aquila faults system. *Quaternary Science Reviews*, *29*(27–28), 3768–3789. <https://doi.org/10.1016/j.quascirev.2010.08.018>
- Galli, P., Giaccio, B., Peronace, E., & Messina, P. (2015). Holocene paleoearthquakes and early–late pleistocene slip rate on the Sulmona fault (central Apennines, Italy). *Bulletin of the Seismological Society of America*, *105*(1), 1–13. <https://doi.org/10.1785/0120140029>
- Galli, P., Messina, P., Peronace, E., Galderisi, A., Ilardo, I., & Polpetta, F. (2023). Paleoseismic evidence of five magnitude 7 earthquakes on the Norcia fault system in the past 8,000 years (Central Italy). *Frontiers in Earth Science*, *11*, 1188602. <https://doi.org/10.3389/feart.2023.1188602>
- Galli, P., Peronace, E., Brammerini, F., Castenetto, S., Naso, G., Cassone, F., & Pallone, F. (2016). The MCS intensity distribution of the devastating 24 August 2016 earthquake in central Italy (M_w 6.2). *Annals of Geophysics*, *59*, 1–3. <https://doi.org/10.4401/ag-7287>
- Galli, P., Peronace, E., & Messina, P. (2022). Archaeoseismic evidence of surface faulting in 1703 Norcia earthquake (Central Italian Apennines, Mw 6.9). *Geosciences*, *12*(1), 14. <https://doi.org/10.3390/geosciences12010014>
- Galli, P. A., Giaccio, B., Messina, P., Peronace, E., & Zuppi, G. M. (2011). Paleoseismology of the L'Aquila faults (central Italy, 2009, M_w 6.3 earthquake): Implications for active fault linkage. *Geophysical Journal International*, *187*(3), 1119–1134. <https://doi.org/10.1111/j.1365-246x.2011.05233.x>
- Gasparini, C., Iannaccone, G., & Scarpa, R. (1985). Fault-plane solutions and seismicity of the Italian peninsula. *Tectonophysics*, *117*(1–2), 59–78. [https://doi.org/10.1016/0040-1951\(85\)90236-7](https://doi.org/10.1016/0040-1951(85)90236-7)

- Gironelli, V., Volatili, T., Luzi, L., Brunelli, G., Zambrano, M., & Tondi, E. (2023). Ground motion simulations of historical earthquakes: The case study of the Fabriano (1741, Mw = 6.1) and Camerino (1799, Mw = 6.1) earthquakes in central Italy. *Bulletin of Earthquake Engineering*, 21(13), 1–22. <https://doi.org/10.1007/s10518-023-01759-y>
- Gori, S., Giaccio, B., Galadini, F., Falcucci, E., Messina, P., Sposato, A., & Dramis, F. (2011). Active normal faulting along the Mt. Morrone south-western slopes (central Apennines, Italy). *International Journal of Earth Sciences*, 100(1), 157–171. <https://doi.org/10.1007/s00531-009-0505-6>
- Guidoboni, E., Ferrari, G., Mariotti, D., Comastri, A., Tarabusi, G., Sgattoni, G., & Valensise, G. (2018). *CFT15Med, Catalogo dei Forti Terremoti in Italia (461 a.C.-1997) e nell'area Mediterranea (760 a.C.-1500)*. Istituto Nazionale di Geofisica e Vulcanologia (INGV). <https://doi.org/10.6092/ingv.it-ctfi5>
- Guidoboni, E., Ferrari, G., Tarabusi, G., Sgattoni, G., Comastri, A., Mariotti, D., et al. (2019). CFT15Med, the new release of the catalogue of strong earthquakes in Italy and in the Mediterranean area. *Scientific Data*, 6(1), 80. <https://doi.org/10.1038/s41597-019-0091-9>
- Gupta, A., & Scholz, C. H. (2000). A model of normal fault interaction based on observations and theory. *Journal of Structural Geology*, 22(7), 865–879. [https://doi.org/10.1016/s0191-8141\(00\)00011-0](https://doi.org/10.1016/s0191-8141(00)00011-0)
- Hardebeck, J. L., Nazareth, J. J., & Hauksson, E. (1998). The static stress change triggering model: Constraints from two southern California aftershock sequences. *Journal of Geophysical Research*, 103(B10), 24427–24437. <https://doi.org/10.1029/98jb00573>
- Harris, R. A., & Simpson, R. W. (1992). Changes in static stress on southern California faults after the 1992 Landers earthquake. *Nature*, 360(6401), 251–254. <https://doi.org/10.1038/360251a0>
- Hetzfel, R., & Hampel, A. (2005). Slip rate variations on normal faults during glacial–interglacial changes in surface loads. *Nature*, 435(7038), 81–84. <https://doi.org/10.1038/nature03562>
- Iezzi, F., Francescone, M., Pizzi, A., Blumetti, A., Boncio, P., Di Manna, P., et al. (2023). Slip localization on multiple fault splays accommodating distributed deformation across normal fault complexities. *Tectonophysics*, 868, 230075. <https://doi.org/10.1016/j.tecto.2023.230075>
- Iezzi, F., Roberts, G., Walker, J. F., & Papanikolaou, I. (2019). Occurrence of partial and total coseismic ruptures of segmented normal fault systems: Insights from the Central Apennines, Italy. *Journal of Structural Geology*, 126, 83–99. <https://doi.org/10.1016/j.jsg.2019.05.003>
- Improta, L., Latorre, D., Margheriti, L., Nardi, A., Marchetti, A., Lombardi, A. M., et al. (2019). Multi-segment rupture of the 2016 Amatrice–Visso–Norcia seismic sequence (central Italy) constrained by the first high-quality catalog of Early Aftershocks. *Scientific Reports*, 9(1), 6921. <https://doi.org/10.1038/s41598-019-43393-2>
- ISIDe Working Group. (2007). *Italian Seismological Instrumental and Parametric Database (ISIDe)*. Istituto Nazionale di Geofisica e Vulcanologia (INGV). <https://doi.org/10.13127/ISIDe>
- ITHACA Working Group. (2019). *ITHACA (ITaly HAZard from CAPable faulting), a database of active capable faults of the Italian territory*. Version December 2019. ISPRA Geological Survey of Italy. Retrieved from <http://sgi2.isprambiente.it/ithacaweb/Mappatura.aspx>
- King, G. C., Stein, R. S., & Lin, J. (1994). Static stress changes and the triggering of earthquakes. *Bulletin of the Seismological Society of America*, 84(3), 935–953.
- Lin, J., & Stein, R. S. (2004). Stress triggering in thrust and subduction earthquakes and stress interaction between the southern San Andreas and nearby thrust and strike-slip faults. *Journal of Geophysical Research*, 109(B2), B02303. <https://doi.org/10.1029/2003jb002607>
- Locati, M., Camassi, R., Rovida, A., Ercolani, E., Bernardini, F., Castelli, V., et al. (2022). Database Macrosismico Italiano (DBMI15), versione 4.0 [Dataset]. Istituto Nazionale di Geofisica e Vulcanologia (INGV). <https://doi.org/10.13127/dbmi/dbmi15.4>
- Mai, P. M., & Thingbaijam, K. K. S. (2014). SRCMOD: An online database of finite-fault rupture models. *Seismological Research Letters*, 85(6), 1348–1357. <https://doi.org/10.1785/0220140077>
- Maleki Asayesh, B., Hamzeloo, H., & Zafarani, H. (2019). Coulomb stress changes due to main earthquakes in Southeast Iran during 1981 to 2011. *Journal of Seismology*, 23(1), 135–150. <https://doi.org/10.1007/s10950-018-9797-y>
- Marchandon, M., Vergnolle, M., & Cavalie, O. (2021). Fault interactions in a complex fault system: Insight from the 1936–1997 NE Lut earthquake sequence. *Geophysical Journal International*, 224(2), 1157–1173. <https://doi.org/10.1093/gji/ggaa451>
- Materazzi, M., Bufalini, M., Dramis, F., Pambianchi, G., Gentili, B., & Di Leo, M. (2022). Active tectonics and paleoseismicity of a transverse lineament in the Fabriano valley, Umbria–Marche Apennine (central Italy). *International Journal of Earth Sciences*, 111(5), 1539–1549. <https://doi.org/10.1007/s00531-022-02198-x>
- Messina, P., Galadini, F., Galli, P., & Sposato, A. (2002). Quaternary basin evolution and present tectonic regime in the area of the 1997–1998 Umbria–Marche seismic sequence (central Italy). *Geomorphology*, 42(1–2), 97–116. [https://doi.org/10.1016/s0169-555x\(01\)00077-0](https://doi.org/10.1016/s0169-555x(01)00077-0)
- Mildon, Z. K., Roberts, G. P., Faure Walker, J. P., & Iezzi, F. (2017). Coulomb stress transfer and fault interaction over millennia on non-planar active normal faults: The Mw 6.5–5.0 seismic sequence of 2016–2017, central Italy. *Geophysical Journal International*, 210(2), 1206–1218. <https://doi.org/10.1093/gji/ggx213>
- Mildon, Z. K., Roberts, G. P., Faure Walker, J. P., & Toda, S. (2019). Coulomb pre-stress and fault bends are ignored yet vital factors for earthquake triggering and hazard. *Nature Communications*, 10(1), 2744. <https://doi.org/10.1038/s41467-019-10520-6>
- Mildon, Z. K., Roberts, G. P., Faure Walker, J. P., Wedmore, L., & McCaffrey, K. J. W. (2016). Active normal faulting during the 1997 seismic sequence in Colfiorito, Umbria: Did slip propagate to the surface? *Journal of Structural Geology*, 91, 102–113. <https://doi.org/10.1016/j.jsg.2016.08.011>
- Mildon, Z. K., Toda, S., Faure Walker, J. P., & Roberts, G. P. (2016). Evaluating models of Coulomb stress transfer: Is variable fault geometry important? *Geophysical Research Letters*, 43(24), 12–407. <https://doi.org/10.1002/2016gl071128>
- Morewood, N. C., & Roberts, G. P. (2000). The geometry, kinematics and rates of deformation within an en echelon normal fault segment boundary, central Italy. *Journal of Structural Geology*, 22(8), 1027–1047. [https://doi.org/10.1016/s0191-8141\(00\)00030-4](https://doi.org/10.1016/s0191-8141(00)00030-4)
- Moro, M., Gori, S., Falcucci, E., Saroli, M., Galadini, F., & Salvi, S. (2013). Historical earthquakes and variable kinematic behaviour of the 2009 L'Aquila seismic event (central Italy) causative fault, revealed by paleoseismological investigations. *Tectonophysics*, 583, 131–144. <https://doi.org/10.1016/j.tecto.2012.10.036>
- Nostro, C., Chiaraluze, L., Cocco, M., Baumont, D., & Scotti, O. (2005). Coulomb stress changes caused by repeated normal faulting earthquakes during the 1997 Umbria–Marche (central Italy) seismic sequence. *Journal of Geophysical Research*, 110(B5), B05S20. <https://doi.org/10.1029/2004jb003386>
- Oskin, M., Perg, L., Shelef, E., Strane, M., Gurney, E., Singer, B., & Zhang, X. (2008). Elevated shear zone loading rate during an earthquake cluster in eastern California. *Geology*, 36(6), 507–510. <https://doi.org/10.1130/g24814a.1>
- Pantosti, D., & Boncio, P. (2012). Understanding the April 6th, 2009, L'Aquila earthquake—the geological contribution: An introductory note to the special issue. *Italian Journal of Geosciences*, 131(3), 303–308. <https://doi.org/10.3301/ijg.2012.25>
- Papanikolaou, I. D., & Roberts, G. P. (2007). Geometry, kinematics, and deformation rates along the active normal fault system in the southern Apennines: Implications for fault growth. *Journal of Structural Geology*, 29(1), 166–188. <https://doi.org/10.1016/j.jsg.2006.07.009>

- Papanikolaou, I. D., Roberts, G. P., & Michetti, A. M. (2005). Fault scarps and deformation rates in Lazio–Abruzzo, Central Italy: Comparison between geological fault slip-rate and GPS data. *Tectonophysics*, *408*(1–4), 147–176. <https://doi.org/10.1016/j.tecto.2005.05.043>
- Pino, N. A., Convertito, V., & Madariaga, R. (2019). Clock advance and magnitude limitation through fault interaction: The case of the 2016 central Italy earthquake sequence. *Scientific Reports*, *9*(1), 5005. <https://doi.org/10.1038/s41598-019-41453-1>
- Reasenber, P. A., & Simpson, R. W. (1992). Response of regional seismicity to the static stress change produced by the Loma Prieta earthquake. *Science*, *255*(5052), 1687–1690. <https://doi.org/10.1126/science.255.5052.1687>
- Roberts, G. P. (2008). Visualisation of active normal fault scarps in the Apennines, Italy: A key to assessment of tectonic strain release and earthquake rupture. *Journal of the Virtual Explorer*, *29*(4). <https://doi.org/10.3809/jvirtex.2008.00197>
- Roberts, G. P., & Michetti, A. M. (2004). Spatial and temporal variations in growth rates along active normal fault systems: An example from The Lazio–Abruzzo Apennines, central Italy. *Journal of Structural Geology*, *26*(2), 339–376. [https://doi.org/10.1016/s0191-8141\(03\)00103-2](https://doi.org/10.1016/s0191-8141(03)00103-2)
- Rovida, A., Locati, M., Camassi, R., Lolli, B., Gasperini, P., & Antonucci, A. (2022). Catalogo Parametrico dei Terremoti Italiani CPTI15, versione 4.0.
- Rubinstein, J. L., Ellsworth, W. L., Chen, K. H., & Uchida, N. (2012). Fixed recurrence and slip models better predict earthquake behavior than the time-and slip-predictable models: 1. Repeating earthquakes. *Journal of Geophysical Research*, *117*(B2), B02306. <https://doi.org/10.1029/2011jb008724>
- Scholz, C. H. (2019). *The mechanics of earthquakes and faulting*. Cambridge University Press.
- Scognamiglio, L., Tinti, E., & Quintiliani, M. (2006). Time Domain Moment Tensor (TDMT) [Dataset]. Istituto Nazionale di Geofisica e Vulcanologia (INGV). <https://doi.org/10.13127/TDMT>
- Shan, B., Xiong, X., Wang, R., Zheng, Y., & Yang, S. (2013). Coulomb stress evolution along Xianshuihe–Xiaojiang Fault System since 1713 and its interaction with Wenchuan earthquake, May 12, 2008. *Earth and Planetary Science Letters*, *377*, 199–210. <https://doi.org/10.1016/j.epsl.2013.06.044>
- Shimazaki, K., & Nakata, T. (1980). Time-predictable recurrence model for large earthquakes. *Geophysical Research Letters*, *7*(4), 279–282. <https://doi.org/10.1029/gl007i004p00279>
- Stein, R. S. (1999). The role of stress transfer in earthquake occurrence. *Nature*, *402*(6762), 605–609. <https://doi.org/10.1038/45144>
- Stein, R. S., Barka, A. A., & Dieterich, J. H. (1997). Progressive failure on the North Anatolian fault since 1939 by earthquake stress triggering. *Geophysical Journal International*, *128*(3), 594–604. <https://doi.org/10.1111/j.1365-246x.1997.tb05321.x>
- Stucchi, M., Monachesi, G., & Mandrelli, F. M. (1991). Investigation of 18th century seismicity in central Italy in the light of the 1741 Fabriano earthquake. *Tectonophysics*, *193*(1–3), 65–82. [https://doi.org/10.1016/0040-1951\(91\)90189-y](https://doi.org/10.1016/0040-1951(91)90189-y)
- The MathWorks Inc. (2022). *MATLAB version: 9.14.0.2137306 (R2023a) Prerelease*. The MathWorks Inc. Retrieved from <https://www.mathworks.com>
- Toda, S., Stein, R. S., Richards-Dinger, K., & Bozkurt, S. B. (2005). Forecasting the evolution of seismicity in southern California: Animations built on earthquake stress transfer. *Journal of Geophysical Research*, *110*(B5), B05S16. <https://doi.org/10.1029/2004jb003415>
- Tondi, E. (2000). Geological analysis and seismic hazard in the central Apennines (Italy). *Journal of Geodynamics*, *29*(3–5), 517–533. [https://doi.org/10.1016/s0264-3707\(99\)00048-4](https://doi.org/10.1016/s0264-3707(99)00048-4)
- Tondi, E., & Cello, G. (2003). Spatiotemporal evolution of the Central Apennines fault system (Italy). *Journal of Geodynamics*, *36*(1–2), 113–128. [https://doi.org/10.1016/s0264-3707\(03\)00043-7](https://doi.org/10.1016/s0264-3707(03)00043-7)
- Tondi, E., Jablonská, D., Volatili, T., Michele, M., Mazzoli, S., & Pierantoni, P. P. (2020). The Campotosto linkage fault zone between the 2009 and 2016 seismic sequences of central Italy: Implications for seismic hazard analysis. *GSA Bulletin*, *133*(7–8), 1679–1694. <https://doi.org/10.1130/b35788.1>
- Valentini, G., Volatili, T., Galli, P., & Tondi, E. (2023). New methodological approach in the evaluation of faults interaction: Insights from the central Apennine fault system. *Bulletin of Geophysics and Oceanography*, *64*(4), 387–404.
- Valoroso, L., Chiaraluce, L., Piccinini, D., Di Stefano, R., Schaff, D., & Waldhauser, F. (2013). Radiography of a normal fault system by 64,000 high-precision earthquake locations: The 2009 L'Aquila (central Italy) case study. *Journal of Geophysical Research: Solid Earth*, *118*(3), 1156–1176. <https://doi.org/10.1002/jgrb.50130>
- Vannoli, P., Burrato, P., Fracassi, U., & Valensise, G. (2012). A fresh look at the seismotectonics of the Abruzzi (Central Apennines) following the 6 April 2009 L'Aquila earthquake (Mw 6.3). *Italian Journal of Geosciences*, *131*(3), 309–329. <https://doi.org/10.3301/ijg.2012.03>
- Vannucci, G., Lolli, B., & Gasperini, P. (2021). Inhomogeneity of macroseismic intensities in Italy and consequences for macroseismic magnitude estimation. *Seismological Research Letters*, *92*(4), 2234–2244. <https://doi.org/10.1785/0220200273>
- Vittori, E., Deiana, G., Esposito, E., Ferrel, L., Marchegiani, L., Mastrolorenzo, G., et al. (2000). Ground effects and surface faulting in the September–October 1997 Umbria–Marche (Central Italy) seismic sequence. *Journal of Geodynamics*, *29*(3–5), 535–564. [https://doi.org/10.1016/s0264-3707\(99\)00056-3](https://doi.org/10.1016/s0264-3707(99)00056-3)
- Walters, R. J., Elliott, J. R., D'agostino, N., England, P. C., Hunstad, I., Jackson, J. A., et al. (2009). The 2009 L'Aquila earthquake (central Italy): A source mechanism and implications for seismic hazard. *Geophysical Research Letters*, *36*(17), L17312. <https://doi.org/10.1029/2009gl013937>
- Wang, L., Gao, H., Feng, G., & Xu, W. (2018). Source parameters and triggering links of the earthquake sequence in central Italy from 2009 to 2016 analyzed with GPS and InSAR data. *Tectonophysics*, *744*, 285–295. <https://doi.org/10.1016/j.tecto.2018.07.013>
- Wedmore, L. N. J., Faure Walker, J. P., Roberts, G. P., Sammonds, P. R., McCaffrey, K. J. W., & Cowie, P. A. (2017). A 667 year record of coseismic and interseismic Coulomb stress changes in central Italy reveals the role of fault interaction in controlling irregular earthquake recurrence intervals. *Journal of Geophysical Research: Solid Earth*, *122*(7), 5691–5711. <https://doi.org/10.1002/2017jb014054>
- Wilkinson, M., Roberts, G. P., McCaffrey, K., Cowie, P. A., Walker, J. P. F., Papanikolaou, I., et al. (2015). Slip distributions on active normal faults measured from LiDAR and field mapping of geomorphic offsets: An example from L'Aquila, Italy, and implications for modelling seismic moment release. *Geomorphology*, *237*, 130–141. <https://doi.org/10.1016/j.geomorph.2014.04.026>
- Xiong, W., Tan, K., Qiao, X., Liu, G., Nie, Z., & Yang, S. (2017). Coseismic, postseismic and interseismic Coulomb stress evolution along the Himalayan main frontal thrust since 1803. *Pure and Applied Geophysics*, *174*(5), 1889–1905. <https://doi.org/10.1007/s00024-017-1525-y>
- Zechar, J. D., & Nadeau, R. M. (2012). Predictability of repeating earthquakes near Parkfield, California. *Geophysical Journal International*, *190*(1), 457–462. <https://doi.org/10.1111/j.1365-246x.2012.05481.x>